5×10^5 DA/3 mammary adenocarcinoma cells, and the development of the tumor growth was scored as above.

Angiogenesis in Matrigel Plugs. Angiogenesis was assessed in Matrigel plugs (25). Mice were inoculated s.c. in the interscapular area with 0.4 ml of Matrigel alone or with Matrigel mixed with 2×10^5 tumor cells. Matrigel is liquid at 4°C but solid at room temperature. In some experiments, recombinant IL-1α or IL-1Ra was added to the mixture of Matrigel and B16 melanoma cells at 4°C just before injection into mice. Saline was mixed with Matrigel to compensate for the volume of IL-1Ra or IL-1α. Matrigel plugs were surgically removed on day 7. Part of each plug was fixed with 10% (vol/vol) formaldehyde, embedded in paraffin, sectioned, and either stained with hematoxylin/eosin or immunostained with antibodies for Von Willebrand's factor, a marker for endothelial cells (26).

Quantification of Microvessel Density (MVD). Microvessels in Matrigel plugs were visualized by using rat antibodies to human Von Willebrand's factor (DAKO), which crossreact with murine Von Willebrand's factor. MVD was determined by first screening areas of highest vascularity under low magnification (×100; ref. 27). The MVD was calculated by counting six highly vascularized fields in each section at a magnification of ×200. MVD calculations were performed by the same pathologist in a blinded manner.

Culture of Peritoneal Macrophages. Peritoneal exudate cells (PEC) were obtained from mice as described (28). Briefly, mice were injected i.p. with thioglycollate (Hy-Labs, Kiryat Weizmann, Rehovot, Israel). After 4 days, PEC were collected from peritoneal lavage and plated (5×10^5 cells per ml) in 24-well plates (Greiner, Frickenhausen, Germany) for 18 h to allow for adherence. Cells were washed, and adherent cell monolayers were activated with B16 melanoma cells (melanoma/macrophage ratio, 1:5). Levels of vascular endothelial cell growth factor (VEGF) and tumor necrosis factor α (TNFα) in 48-h supernatants were measured by specific ELISA kits (DuoSet, R & D Systems).

Results

Tumorigenicity of B16 Melanoma Cells in IL-1β KO Mice. Tumor growth was assessed in C57BL/6 WT mice and in IL-1β KO mice from the same background. Because B16 melanoma cells metastasize to the lungs, the development of experimental lung metastasis after i.v. inoculation of the malignant cells and mortality was recorded. Consistently, as shown in Fig. 1*A*, all WT C57BL/6 mice died within 20 days, whereas all IL-1β KO mice injected with the B16 cells remained alive throughout the experiment. Mice died from lung metastasis (Fig. 1*B*), as evidenced in histological sections from moribund mice suffering from dyspnea. To evaluate the kinetics of local tumor development in IL-1β KO, B16 melanoma cells were injected i.f.p., and the diameter of the tumors was measured every 5 days. As shown in Fig. 1*C*, no tumor development was observed when B16 melanoma cells were injected into IL-1β KO mice, whereas progressive tumor growth was observed in WT mice. In F_1 (WT × IL-1β KO) of C57BL/6 origin tumors developed as in WT mice (data not shown).

Reduced *in Vivo* Angiogenesis of B16 Melanoma Tumors in IL-1β KO Mice. Next, we examined the *in vivo* recruitment of the angiogenic network into Matrigel plugs embedded with B16 melanoma cells. Tumor cells were mixed with Matrigel and injected s.c. into WT and IL-1β KO mice. As shown in Fig. 2 *Upper Inset*, active angiogenesis could be observed macroscopically in plugs recovered from WT mice: the plugs are more red compared with B16 melanoma cell-containing plugs from IL-1β KO mice (Fig. 2

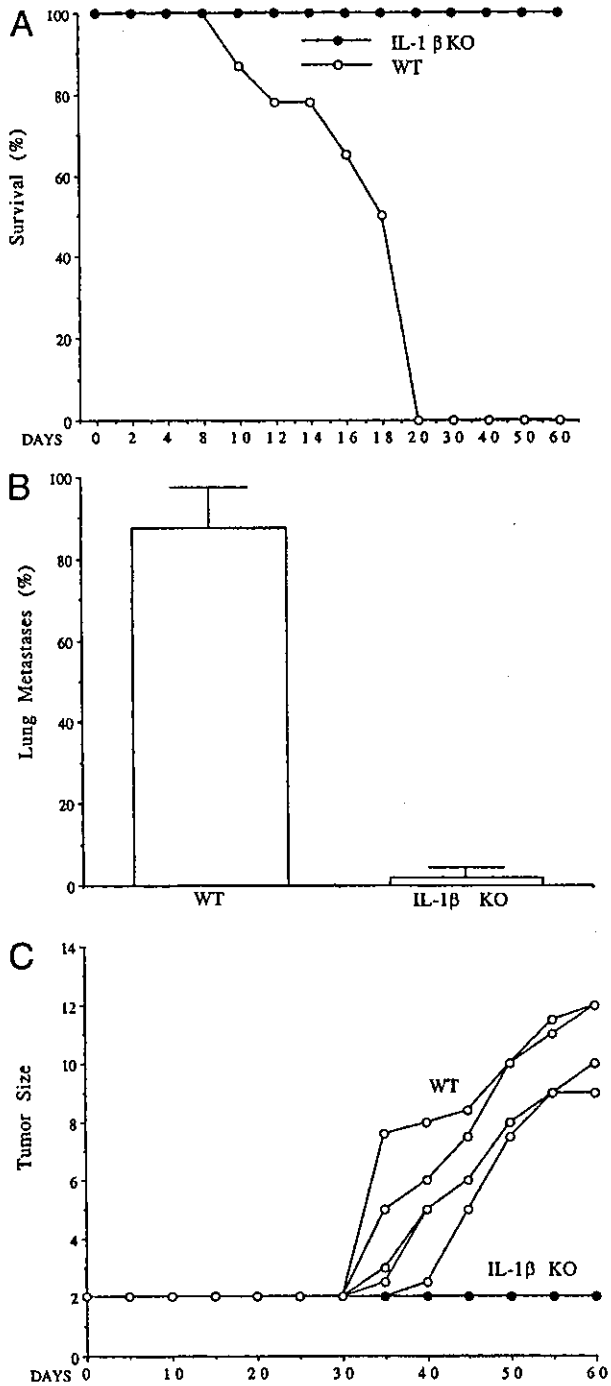

Fig. 1. Increased survival rate and decreased tumor growth in IL-1β KO mice. (*A*) Survival after i.v. injection of B16 melanoma into IL-1β KO (n = 10) compared with WT mice (n = 10). (*B*) Frequency of lung micrometastases as detected in histological sections on day 14 after tumor cell injection (n = 10). (*C*) Tumor size of B16 melanoma after i.f.p. injection (2×10^5 cells per mouse; n = 5 per group). Results shown are from one experiment of six performed.

Lower Inset). To directly view angiogenesis in the plugs, histological sections were stained with antibodies against Von Willebrand's factor. As shown in Fig. 2, B16 melanoma cells embedded in Matrigel plugs in WT mice induced a potent angiogenic response (*Upper*), whereas the angiogenic response

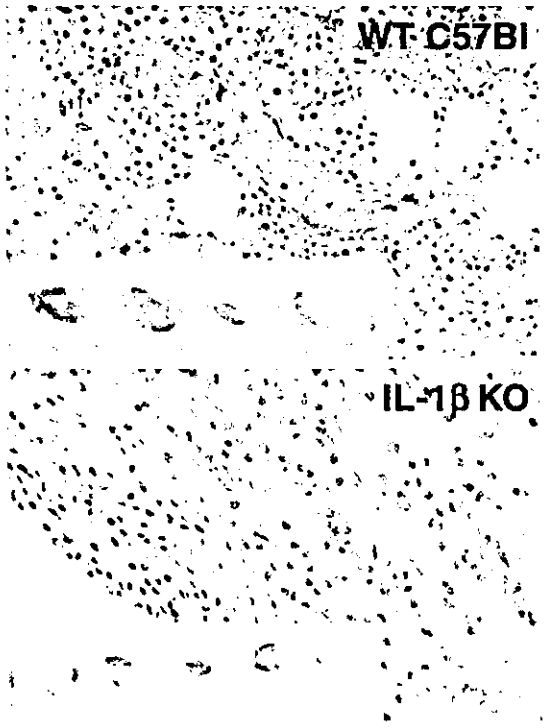

Fig. 2. Blood vessel growth in B16 cells embedded in Matrigel plugs. (*Upper*) Section through a B16-embedded Matrigel plug injected s.c. in WT mice and removed on day 7 (×400). (*Inset*) Gross morphology of Matrigel plugs. (*Lower*) Similarly stained sections through Matrigel plugs injected into IL-1β KO mice. Results shown are from one of four experiments performed.

developing in malignant cells containing plugs from IL-1β KO mice exhibited a background response.

IL-1 Controls Tumor Angiogenesis. To study whether IL-1 is indeed the factor responsible for this tumor-induced angiogenic response, Matrigel plugs injected into IL-1β KO mice were supplemented with IL-1, in this case, recombinant murine IL-1α. As depicted in Fig. 3*A*, recombinant IL-1α embedded into Matrigel plugs together with B16 melanoma cells before gelation largely restored the missing angiogenic response observed in IL-1β KO mice.

Next, increasing concentrations of IL-1Ra were incorporated into B16 melanoma-containing Matrigel plugs and injected into WT mice. This procedure resulted in a dose-dependent reduction in MVD in the plugs (Fig. 3*B*). Together, these results demonstrate that microenvironmental IL-1β is required for tumor invasiveness, possibly through induction of an angiogenic response.

Because recombinant IL-1α substituted the angiogenic response missing in IL-1β KO mice, it was of interest to assess directly the effects of microenvironmental IL-1α on tumor invasiveness and blood vessel formation. B16 melanoma cells were injected i.f.p. into WT, IL-1α, or IL-1β KO C57BL/6 mice, and the growth of local tumors was determined. Again, in IL-1β KO mice, no tumor development was observed, whereas in WT mice, B16 melanoma induced progressive tumors. In IL-1α KO mice, tumorigenicity patterns of B16 cells were reduced compared with the WT mice, as evidenced by the late appearance and slower growth rate of the tumors (Fig. 4*A*). Next, the angiogenic response in B16 melanoma-containing Matrigel plugs from WT, IL-1α, and IL-1β KO mice was compared. As shown by MVD in Fig. 4*B*, in IL-1β KO mice, the angiogenic

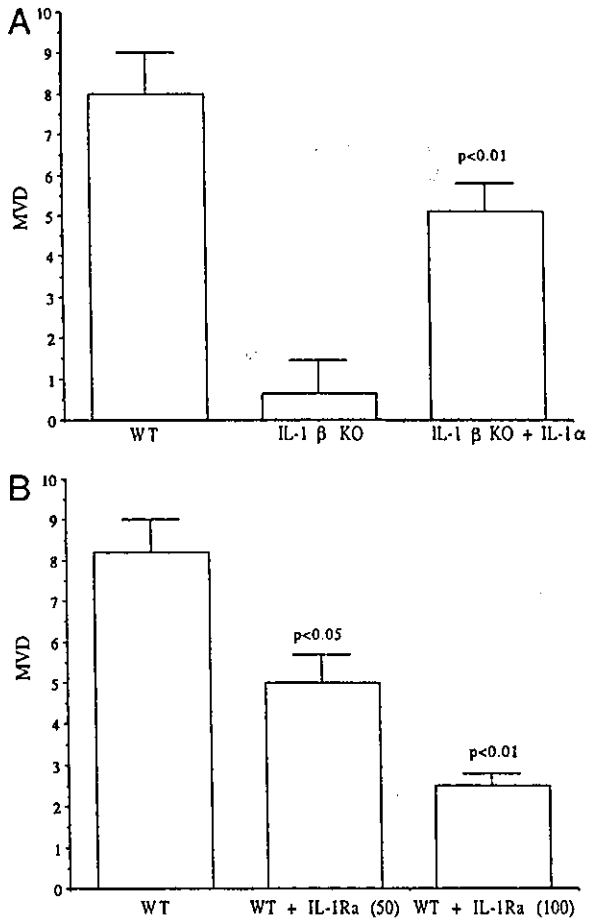

Fig. 3. MVD in B16 melanoma embedded in Matrigel plugs. (*A*) MVD ± SEM in B16 melanoma-embedded Matrigel plugs in WT or IL-1β KO mice on day 7. IL-1β KO mice were also implanted with Matrigel plugs embedded with a mixture of B16 cells and 100 ng of murine IL-1α per 0.4 ml of Matrigel (n = 5 in each group). (*B*) Day 7 MVD of Matrigel plugs embedded into WT mice containing a mixture of B16 melanoma cells plus saline, 50 or 100 μg of recombinant human IL-1Ra per 0.4 ml of Matrigel (n = 5 in each group).

response is nearly absent, whereas in IL-1α KO mice, the response is reduced by ≈50%, compared with that in WT mice.

Effects of IL-1 on Tumor Invasiveness and Angiogenesis in DA/3 Mammary Adenocarcinoma Tumors. It was necessary to determine whether host-derived IL-1 also affects the *in vivo* growth patterns of other experimental tumors. The mammary cancer tumor DA/3 in BALB/c mice was used. As shown in Fig. 5*A*, in IL-1α KO mice, no tumor development was observed, whereas in IL-1β KO mice, tumors developed slower and were smaller compared with tumors in WT BALB/c mice. This hierarchy was also observed when MVD was determined on sections from Matrigel plugs containing embedded DA/3 cells in control, IL-1α KO, and IL-1β KO BALB/c mice (Fig. 5*B*). It seems that host-derived IL-1 is important for the growth of both B16 melanoma and DA/3 breast cancer cells. For B16 cells, IL-1β plays a dominant role in tumor development; for the invasiveness of DA/3 cells, IL-1α plays a more dominant role.

Role of IL-1 in the Production of VEGF and TNFα from PEC. Upon interaction with malignant cells, macrophages present in the tumor's microenvironment likely secrete factors that may

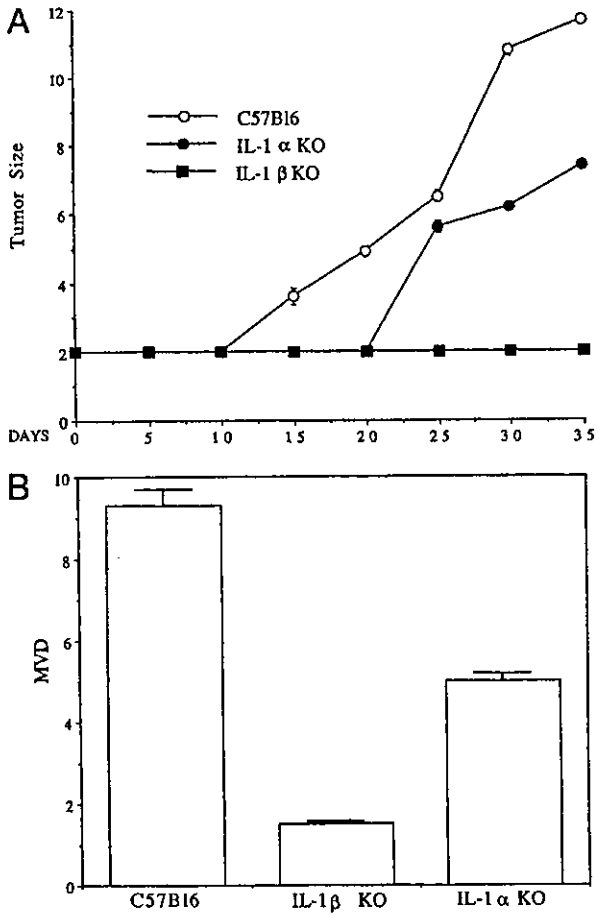

Fig. 4. Growth and MVD of B16 melanoma cells in WT, IL-1α, and IL-1β KO mice. (*A*) Tumor growth in mice injected i.f.p. with B16 cells, as indicated in legend to Fig. 1C. The results represent one of three experiments. Mean ± SEM for each (n = 8 per group) are shown. (*B*) MVD ± SEM in B16 melanoma-embedded Matrigel plugs (2×10^5) in WT, IL-1β, or IL-1α KO mice (n = 5 in each group).

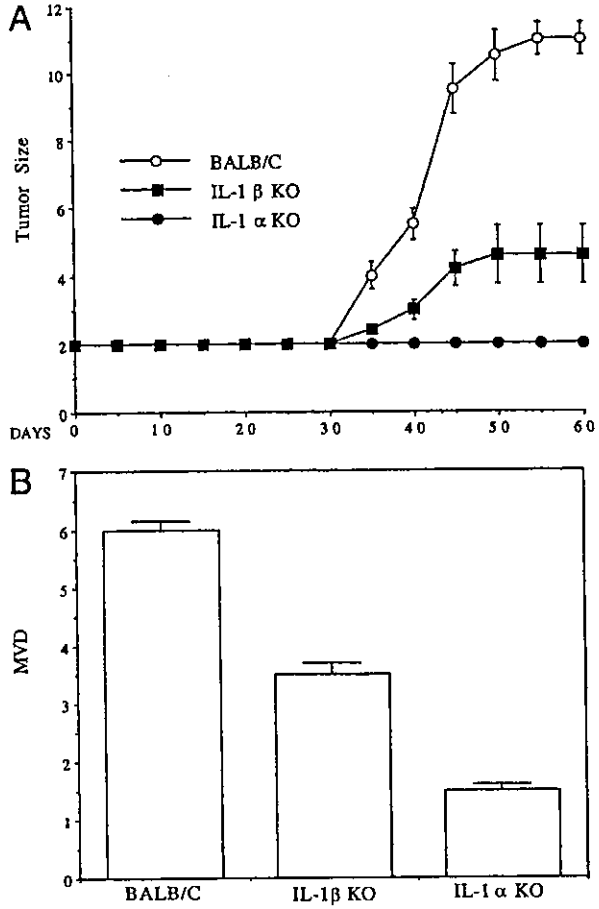

Fig. 5. Growth and MVD of DA/3 mammary cancer cells in WT BALB/c, IL-1α, or IL-1β KO mice. (*A*) Mice were injected i.f.p. with DA/3 cells (5×10^5 cells per mouse). The results represent one of three experiments. Mean ± SEM from each group (n = 8 per group) are shown. (*B*) MVD ± SEM in DA/3-embedded Matrigel plugs (2×10^5) in WT, IL-1β, or IL-1α KO mice (n = 5 in each group).

affect the malignant process, including tumor angiogenesis. Thus, we assessed the production of VEGF in macrophages from control and IL-1 KO mice that were cocultured with B16 melanoma cells. Adherent PEC were incubated with melanoma cells for 48 h, and the supernatants were assessed for VEGF and TNFα. Cultured alone, PEC did not release VEGF or TNFα. In contrast, melanoma cells cultured alone released 20 pg/ml VEGF but not TNFα after 48 h (not shown). In cocultures of peritoneal macrophages from WT mice plus B16 cells (as shown in Fig. 6), a further increase in VEGF secretion was observed; however, this increase was reduced by ≈50% when macrophages were obtained from IL-1β KO or IL-1α KO mice. In macrophage-B16 cocultures, TNFα (Fig. 7) and IL-6 (not shown), were also induced; their generation was largely inhibited by IL-1Ra. As can be seen in Fig. 7, less TNFα was observed in supernatants of cocultures consisting of macrophages from IL-1β KO mice, and in both cases TNFα release was inhibited by IL-1Ra.

Discussion

The present study demonstrates the role of endogenous IL-1 in promoting the invasiveness of malignant cells and emphasizes the dependency of tumor angiogenesis on this cytokine. To our knowledge, this is the first report that shows that mostly IL-1β accounts for the ability of tumor cells to initiate and complete the processes of angiogenesis, as manifested by the inability of tumor cells embedded in Matrigel plugs to recruit a vasculature network. Mice solely deficient in IL-1α or IL-1β exhibit dramatically impaired tumor development and blood vessel growth. These findings seem to represent a general phenomenon, because they were observed in different experimental tumor models: B16 melanoma, DA/3 mammary adenocarcinoma in BALB/e mice, and prostate cancer cell lines injected i.f.p. into C57Bl6 mice (data not shown). It seems that for B16 melanoma and prostate cancer, IL-1β is essential for invasiveness, but for others (DA/3 mammary cancer), IL-1α plays a greater role than IL-1β.

B16 melanoma cells injected into the footpad of IL-1β-deficient mice failed to develop into local tumors, compared with WT mice. In IL-1α-deficient mice, the reduction was less dramatic. This failure to proliferate and progress into an expansive tumor is likely caused by an inability to initiate angiogenesis. On histological examination, B16 cells injected into IL-1β-deficient mice remained pigmented at the site of inoculation, similar to their appearance in culture, and thus possibly representing dormant tumor cells. This result was in sharp contrast to control WT mice, where invading B16 melanoma cells seemed to be

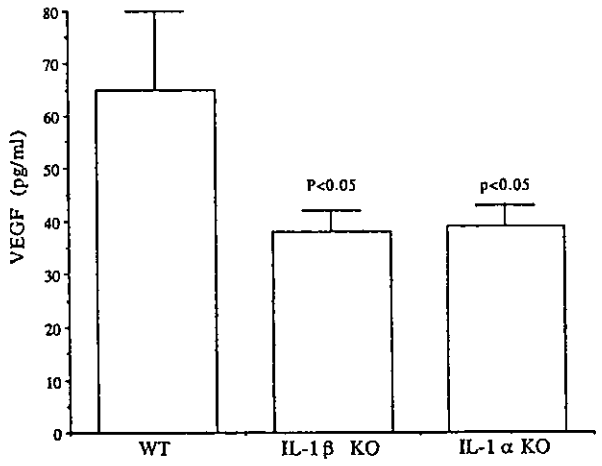

Fig. 6. VEGF secretion in cocultures of B16 melanoma cells and macrophages from WT, IL-1α, or IL-1β KO mice. PEC were obtained and cocultured with B16 melanoma cells, as indicated in *Materials and Methods*. Mean ± SEM VEGF levels in 48-h supernatants were measured (n = 5 experiments).

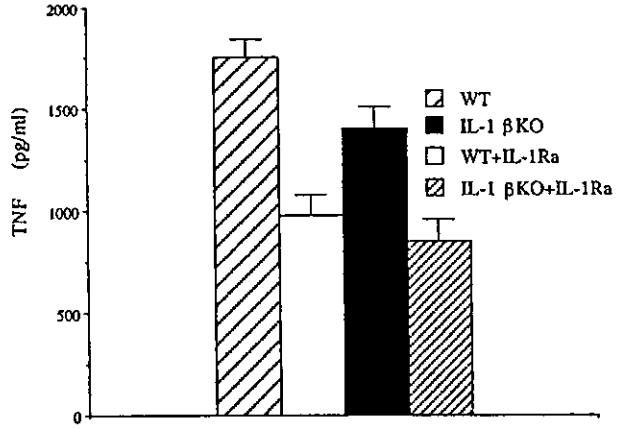

Fig. 7. TNFα secretion in cocultures of B16 melanoma cells and macrophages from WT and IL-1β KO mice. PEC were obtained and stimulated with melanoma cells in the presence or absence of IL-1Ra (10 μg/ml). Mean ± SEM TNFα levels in 48-h supernatants are shown (n = 5 experiments).

de-differentiated and to lose melanin (data not shown). Moreover, when injected i.v., B16 cells produce micrometastases in the lungs, resulting in death after 14–16 days, whereas in IL-1β-deficient mice, micrometastases were not observed, and mice were long survivors, at least 6 months after tumor-cell injection.

We also examined the effect of specific blockade of IL-1 receptor in WT mice by using the IL-1Ra. IL-1Ra incorporated into B16 cell-containing Matrigel plugs implanted into WT mice significantly reduced the outgrowth of tumors and the recruitment of an angiogenic network into the plugs. Furthermore, the addition of 100 ng of recombinant IL-1 into Matrigel plugs with B16 cells in IL-1β KO mice resulted in restoration of the angiogenic response. Thus, the use of IL-1Ra itself, as well as other methods to reduce IL-1 activity, may have clinical utility in both inflammatory as well as neoplastic diseases where angiogenesis is a contributing factor.

Both IL-1α and IL-1β were shown to contribute to tumor angiogenesis and invasiveness, but the role of IL-1β is more evident in these processes. This may be due to IL-1β being secreted into the microenvironment, thus activating cells in the tumor's stroma, including the malignant cells. In contrast, the effects of IL-1α are more limited, as this cytokine is largely cell-associated. The present findings agree with our previous observations that tumor cells engineered to secrete IL-1β result in a more severe and invasive pattern compared with that of mock-transfected cells (15). In contrast, in that study, IL-1α-expressing transfectants did not produce tumors, likely because of IL-1α-induced immune responses, which eradicated the malignant cells (15, 28–30).

We emphasize the role of host-derived IL-1 as an important factor for tumor angiogenesis and tumor growth. Previous studies have focused on the invasion-promoting features of IL-1 (9–12, 14, 17). IL-1 induces adhesion molecule expression on both malignant and endothelial cells (11), enabling access of malignant cells into the circulation and their invasiveness. Vidal-Vanaclocha and coworkers (10, 13, 14, 17) have demonstrated the role of hepatic sinusoidal endothelial cell-derived IL-1 in promoting hepatic metastasis of B16 melanoma cells. In that model, reduction of metastases and increased survival rates were observed using systemic administration of IL-1Ra (10). Hepatic metastasis was also significantly reduced in IL-1β-deficient mice and almost completely absent in mice deficient in the IL-1β-converting enzyme, which processes the precursors of IL-1β as well as IL-18 (17). *In vitro*, increased binding of the melanoma cells to hepatic sinusoidal endothelial cells was observed and shown to be caused by the up-regulation of expression of vascular cell adhesion molecule-1 and possibly other adhesion molecules on endothelial cells (10, 13, 14). Supernatants of melanoma cells stimulated endothelial cells to secrete IL-1β, TNFα, and IL-18, each of which up-regulate adhesion molecule expression.

Multiple cytokines may affect tumor growth by stimulating angiogenic factor production (2–8). The role of IL-1 in inducing VEGF production has been described (31). Moreover, IL-1β selectively induces the expression of hypoxia inducible factor-1α, a dominant transcription factor for VEGF (32–35). Here, we show that endogenous IL-1 is involved in the production of VEGF in cocultures of macrophages and B16 melanoma cells: by using macrophages from IL-1β and IL-1α KO mice, there was reduced VEGF secretion. Nozaki *et al.* (36) have shown that VEGF production by breast cancer cells, which constitutively secrete IL-1α, is not inhibited by anti-IL-1 antibodies, whereas IL-6 and IL-8 are inhibited by these antibodies, suggesting that the effects of IL-1 on VEGF production are indirect. However, IL-1 is directly involved in production of IL-6 and TNFα in cocultures of macrophages and B16 melanoma cells where production of TNFα and IL-6 is lower in macrophages from IL-1β KO mice, and, in each case, inhibited by IL-1Ra.

Intervention in tumor vascularity in experimental tumors has been reported using inhibitors of the VEGF loop (37–39) and anti-angiogenic factors, i.e., angiostatin, endostatin (4–6, 40, 41), and IFN-α or -β (42). In addition, antiproteolytic agents, which target metalloproteinases (43, 44) and heparanase (45), inhibit extra cellular matrix degradation and possess anti-tumor activity. Anti-inflammatory agents, such as cyclooxygenase inhibitors (46) and inhibitors of NF-κB (47, 48), have also been effective in reducing angiogenesis. Because IL-1 is a major inducer of inflammation and particularly of cyclooxygenase-2 (1), other angiogenic and small mediator molecules may represent a downstream event of an IL-1-initiated signal. As such, IL-1 may serve as a master cytokine upon which different angiogenic stimuli converge. Thus, blockade of a single molecule, i.e., IL-1, may inhibit the cascade of downstream (effector) angiogenic factors. In VEGF-impregnated nylon discs implanted into rat corneal stromata,

systemic treatment with IL-1Ra reduced the numbers of new blood vessels growing from the corneal limbus toward the implant by 75% (49). Thus, the use of IL-1Ra, which blocks cell activation by either IL-1β or IL-1α and is approved for reducing inflammation in patients with rheumatoid arthritis, may be an appropriate therapeutic strategy for inhibiting tumor angiogenesis. The use of IL-1Ra as an adjunct therapy in combination with tumor resection and chemotherapy is supported by our preclinical studies.

We thank Rosalyn M. White and Parvin Zarin for skillful technical help and Philip Bufler for advice. R.N.A. is supported by the Israel Ministry of Science jointly with the Deutsches Krebsforschungszentrum (Heidelberg), the United States–Israel Binational Science Foundation, the Israel Science Foundation founded by the Israel Academy of Sciences and Humanities, the Israel Cancer Association, and the Association for International Cancer Research. E.V. is supported by the Concern Foundation, the Israel Cancer Association, and the Israeli Ministry of Health. C.A.D. is supported by National Institutes of Health Grant AI-15614.

1. Dinarello, C. A. (1996) *Blood* **87**, 2095–2147.
2. Folkman, J. (1971) *N. Engl. J. Med.* **285**, 404–405.
3. Folkman, J. (1990) *Cancer Metastasis Rev.* **9**, 171–174.
4. Holmgren, L., O'Reilly, M. S. & Folkman, J. (1995) *Nat. Med.* **1**, 149–153.
5. Folkman, J. & D'Amore, P. A. (1996) *Cell* **87**, 1153–1155.
6. Hanahan, D. & Folkman, J. (1996) *Cell* **86**, 353–364.
7. Carmeliet, P. & Jain, R. K. (2000) *Nature* **407**, 249–257.
8. Liotta, L. A. & Kohn, E. C. (2001) *Nature* **411**, 375–379.
9. Chirivi, R. G., Garofalo, A., Padura, I. M., Mantovani, A. & Giavazzi, R. (1993) *Cancer Res.* **53**, 5051–5054.
10. Vidal-Vanaclocha, F., Amezaga, C., Asumendi, A., Kaplanski, G. & Dinarello, C. A. (1994) *Cancer Res.* **54**, 2667–2672.
11. Chirivi, R. G., Chiodoni, C., Musiani, P., Garofalo, A., Bernasconi, S., Colombo, M. P. & Giavazzi, R. (1996) *Int. J. Cancer* **67**, 856–863.
12. McKenzie, R. C., Oran, A., Dinarello, C. A. & Sauder, D. N. (1996) *Anticancer Res.* **16**, 437–441.
13. Vidal-Vanaclocha, F., Alvarez, A., Asumendi, A., Urcelay, B., Tonino, P. & Dinarello, C. A. (1996) *J. Natl. Cancer Inst.* **88**, 198–205.
14. Anasagasti, M. J., Alvarez, A., Martin, J. J., Mendoza, L. & Vidal-Vanaclocha, F. (1997) *Hepatology* **25**, 840–846.
15. Apte, R. N., Dvorkin, T., Song, X., Fima, E., Krelin, Y., Yulevitch, A., Gurfinkel, R., Werman, A., White, R. M., Argov, S., *et al.* (2000) *Adv. Exp. Med. Biol.* **479**, 277–288.
16. Apte, R. N. & Voronov, E. (2002) *Semin. Cancer Biol.* **12**, 277–290.
17. Vidal-Vanaclocha, F., Fantuzzi, G., Mendoza, L., Fuentes, A. M., Anasagasti, M. J., Martin, J., Carrascal, T., Walsh, P., Reznikov, L. L., Kim, S. H., *et al.* (2000) *Proc. Natl. Acad. Sci. USA* **97**, 734–739.
18. Mantovani, A. & Dejana, E. (1989) *Immunol. Today* **10**, 370–375.
19. Meager, A. (1999) *J. Immunol. Methods* **227**, 197–198.
20. Porgador, A., Tzehoval, E., Katz, A., Vadai, E., Revel, M., Feldman, M. & Eisenbach, L. (1992) *Cancer Res.* **52**, 3679–3686.
21. Fu, Y. X., Watson, G., Jimenez, J. J., Wang, Y. & Lopez, D. M. (1990) *Cancer Res.* **50**, 227–234.
22. Zheng, H., Fletcher, D., Kozak, W., Jiang, M., Hofmann, K. J., Conn, C. A., Soszynski, D., Grabiec, C., Trumbauer, M. E., Shaw, A., *et al.* (1995) *Immunity* **3**, 9–19.
23. Fantuzzi, G., Zheng, H., Faggioni, R., Benigni, F., Ghezzi, P., Sipe, J. D., Shaw, A. R. & Dinarello, C. A. (1996) *J. Immunol.* **157**, 291–296.
24. Horai, R., Asano, M., Sudo, K., Kanuka, H., Suzuki, M., Nishihara, M., Takahashi, M. & Iwakura, Y. (1998) *J. Exp. Med.* **187**, 1463–1475.
25. Fridman, R., Kibbey, M. C., Royce, L. S., Zain, M., Sweeney, M., Jicha, D. L., Yannelli, J. R., Martin, G. R. & Kleinman, H. K. (1991) *J. Natl. Cancer Inst.* **83**, 769–774.
26. Sehested, M. & Hou-Jensen, K. (1981) *Virchows Arch. A Pathol. Anat. Histol.* **391**, 217–225.
27. Weidner, N., Semple, J. P., Welch, W. R. & Folkman, J. (1991) *N. Engl. J. Med.* **324**, 1–8.
28. Voronov, E., Weinstein, Y., Benharroch, D., Cagnano, E., Ofir, R., Dobkin, M., White, R. M., Zoller, M., Barak, V., Segal, S. & Apte, R. N. (1999) *Cancer Res.* **59**, 1029–1035.
29. Douvdevani, A., Huleihel, M., Zoller, M., Segal, S. & Apte, R. N. (1992) *Int. J. Cancer* **51**, 822–830.
30. Apte, R. N., Douvdevani, A., Zoller, M., White, R. M., Dvorkin, T., Shimoni, N., Fima, E., Hacham, M., Huleihel, M., Benharroch, D., *et al.* (1993) *Immunol. Lett.* **39**, 45–52.
31. Saijo, Y., Tanaka, M., Miki, M., Usui, K., Suzuki, T., Maemondo, M., Hong, X., Tazawa, R., Kikuchi, T., Matsushima, K. & Nukiwa, T. (2002) *J. Immunol.* **169**, 469–475.
32. Carmeliet, P., Dor, Y., Herbert, J. M., Fukumura, D., Brusselmans, K., Dewerchin, M., Neeman, M., Bono, F., Abramovitch, R., Maxwell, P., *et al.* (1998) *Nature* **394**, 485–490.
33. Keshet, E. & Ben-Sasson, S. A. (1999) *J. Clin. Invest.* **104**, 1497–1501.
34. Thornton, R. D., Lane, P., Borghaei, R. C., Pease, E. A., Caro, J. & Mochan, E. (2000) *Biochem. J.* **350**, Part 1, 307–312.
35. Haddad, J. J. (2002) *Eur. Cytokine Network* **13**, 250–260.
36. Nozaki, S., Sledge, G. W., Jr., & Nakshatri, H. (2000) *Biochem. Biophys. Res. Commun.* **275**, 60–62.
37. Neufeld, G., Kessler, O., Vadasz, Z. & Gluzman-Poltorak, Z. (2001) *Surg. Oncol. Clin. North Am.* **10**, 339–56, ix.
38. Dor, Y., Djonov, V., Abramovitch, R., Itin, A., Fishman, G. I., Carmeliet, P., Goelman, G. & Keshet, E. (2002) *EMBO J.* **21**, 1939–1947.
39. Harris, A. L. (2002) *Nat. Rev. Cancer* **2**, 38–47.
40. O'Reilly, M. S., Holmgren, L., Shing, Y., Chen, C., Rosenthal, R. A., Moses, M., Lane, W. S., Cao, Y., Sage, E. H. & Folkman, J. (1994) *Cell* **79**, 315–328.
41. O'Reilly, M. S., Boehm, T., Shing, Y., Fukai, N., Vasios, G., Lane, W. S., Flynn, E., Birkhead, J. R., Olsen, B. R. & Folkman, J. (1997) *Cell* **88**, 277–285.
42. Slaton, J. W., Perrotte, P., Inoue, K., Dinney, C. P. & Fidler, I. J. (1999) *Clin. Cancer Res.* **5**, 2726–2734.
43. Kleiner, D. E. & Stetler-Stevenson, W. G. (1999) *Cancer Chemother. Pharmacol.* **43**, Suppl., S42–S51.
44. Zucker, S., Cao, J. & Chen, W. T. (2000) *Oncogene* **19**, 6642–6650.
45. Vlodavsky, I. & Friedmann, Y. (2001) *J. Clin. Invest.* **108**, 341–347.
46. Thun, M. J., Henley, S. J. & Patrono, C. (2002) *J. Natl. Cancer Inst.* **94**, 252–266.
47. Scatena, M. & Giachelli, C. (2002) *Trends Cardiovasc. Med.* **12**, 83–88.
48. Huang, S., Pettaway, C. A., Uehara, H., Bucana, C. D. & Fidler, I. J. (2001) *Oncogene* **20**, 4188–4197.
49. Coxon, A., Bolon, B., Estrada, J., Kaufman, S., Scully, S., Rattan, A., Duryea, D., Hu, Y. L., Rex, K., Pacheco, E., *et al.* (2002) *Arthritis Rheum.* **46**, 2604–2612.

Available online at www.sciencedirect.com
SCIENCE DIRECT®
Neuroscience Research 45 (2003) 313–324
Neuroscience Research
www.elsevier.com/locate/neures

Suppression of oxidative neuronal damage after transient middle cerebral artery occlusion in mice lacking interleukin-1

Hirokazu Ohtaki [a,b], Hisayuki Funahashi [a], Kenji Dohi [a], Takiko Oguro [c], Reiko Horai [d], Masahide Asano [d], Yoichiro Iwakura [d], Li Yin [a], Masaji Matsunaga [a], Noboru Goto [a], Seiji Shioda [a,b,*]

[a] *Department of Anatomy, Showa University School of Medicine, 1-5-8 Hatanodai, Shinagawa-ku, Tokyo 142-8555, Japan*
[b] *The Core Research for Evolutional Science and Technology (CREST) of Japan Science and Technology Corporation (JST), Tokyo, Japan*
[c] *Pharmaceutical Sciences, Showa University, Shinagawa-ku, Tokyo 142-8555, Japan*
[d] *The Institute of Medical Science, Laboratory of Animal Research Center, The University of Tokyo, Minato-ku, Tokyo 108-8639, Japan*

Received 11 September 2002; accepted 19 November 2002

Abstract

Interleukin-1 (IL-1) contributes to ischemic neurodegeneration. However, the mechanisms regulating action of IL-1 are still poorly understood. In order to clear this central issue, mice that were gene deficient in IL-1α and β (IL-1 KO) and wild-type mice were subjected to 1-h transient middle cerebral artery occlusion (tMCAO). Expression levels of IL-1β and IL-1 receptor I (IL-1RI) were then examined. Generation of peroxynitrite and the expression of mRNAs for nitric oxide synthase (NOS) subtypes were also determined. Immunostaining for IL-1β was increased from 6 h and peaked at 24 h after tMCAO in the microglia and macrophage. The immunoreactivities of IL-1RI were increased progressively in the microvasculature and neuron-like cells of the ipsilateral hemisphere. Infarct volumes were significantly lower in IL-1 KO mice compared with wild-type mice 48 h after tMCAO ($P < 0.01$). The immunoreactivities of 3-nitro-L-tyrosine were determined in the neurons and microvasculature 24 h after tMCAO and were significantly decreased in the IL-1 KO mice compared to wild-type mice. In addition, expression levels of NOS mRNA in IL-1 KO mice were lower than that measured in wild-type mice. These results indicate that IL-1 is up-regulated and may play a role in neurodegeneration by peroxynitrite production during ischemia.

Keywords: Interleukin-1 (IL-1); Interleukin-1 receptor I (IL-1RI); Focal brain ischemia; Brain infarction; Microglia; Peroxynitrite (ONOO); Nitric oxide synthase (NOS)

1. Introduction

Interleukin-1 (IL-1) is a proinflammatory cytokine, which plays a crucial role in the host's response to inflammation, infection, injury, and immunological challenge (Durum and Oppenheim, 1993; Van Dam et al., 1995; Dinarello, 1996; Tocci and Schmidt, 1997). IL-1 consists of two molecular species, IL-1α and β, which are derived from two distinct genes located 50 kb apart on chromosome 2 of the mouse genome (D'Eutachio et al., 1987; Silver et al., 1990). IL-1, especially IL-1β has diverse actions in the brain and there is considerable evidence implicating it in neurodegeneration. Injection of IL-1β has been shown to exacerbate ischemic brain damage (Yamasaki et al., 1995; Rothwell, 1999; Touzani et al., 1999) and injection of IL-1 receptor antagonist leads to a decrease in infarct volumes (Relton and Rothwell, 1992; Betz et al., 1995; Garcia et al., 1995; Loddick and Rothwell, 1996; Sanderson et al., 1999; Yang et al., 1999a). However, the mechanisms regulating the action of IL-1 are poorly understood.

There is increasing evidence available to indicate that nitric oxide (NO) may be an important mediator of ischemic brain injury (Hara et al., 1996; Homma et al., 1997; Kamii et al., 1996; Iadecola, 1997). NO is produced by nitric oxide synthase (NOS), and reacts

* Corresponding author. Tel.: +81-3-3784-8103; fax: +81-3-3784-6815.
E-mail address: shioda@med.showa-u.ac.jp (S. Shioda).

0168-0102/02/$ - see front matter
doi:10.1016/S0168-0102(02)00238-9

with the superoxide anion (O_2) to form peroxynitrite ($ONOO^-$), a powerful oxidant, in postischemic reperfusion (Tanaka et al., 1997; Fukuyama et al., 1998). $ONOO^-$ directly oxidizes sulfhydryl groups in L-tyrosine and there by alters or prevents the normal functioning of those proteins. Although it is difficult to detect $ONOO^-$, 3-nitro-L-tyrosine (3-NT), the reaction product of $ONOO^-$ can be detected using immunohistochemical techniques and is considered to be a reliable marker for $ONOO^-$. On the other hand, the addition of IL-1β into cultured human microglia and rat microvascular endothelial cells express inducible NOS (iNOS) mRNA and generate NO (Bonmann et al., 1997; Ding et al., 1997). These results suggest that NO and $ONOO^-$ formation may be associated with the neurodegenerative mechanism of IL-1 after ischemia/reperfusion. However, the relationship between IL-1 and $ONOO^-$ formation after ischemia is still unclear.

Thus, the purpose of the present work is to determine the neurodegenerative mechanism of IL-1 to focus on the generation of $ONOO^-$ and NOS after transient ischemia.

2. Materials and methods

2.1. Mice

Mice with homozygous disruption of both IL-1α and β genes (IL-1 KO) have been described previously (Horai et al., 1998). IL-1 KO mice that had been backcrossed for six to nine generations into BALB/c strain were used in these experiments. Wild-type mice were generated from the same chimeric founder. The mice were raised in the specific pathogen-free animal facility at Showa University, with a 12-h light/dark cycle and had free access to food and water. All experimental procedures involving animals were approved by the Institutional Animal Care and Use Committee of Showa University.

2.2. Production of transient middle cerebral artery occlusion

Adult male mice weighing 24–27.5 g (8–12 wk) were subjected to focal cerebral ischemia. Anesthesia was induced by inhalation of 4.0% sevoflurane and maintained by inhalation of 2.0% sevoflurane in N_2O/O_2 (70/30%) through a facemask. Body temperature was monitored with a rectal thermometer and maintained at 36.5–37.5 °C by a heating blanket. Ischemia was induced by occlusion of the left middle cerebral artery (MCA) using the intraluminal filament technique. Left common carotid artery (CCA) was exposed through a midline incision. External carotid artery (ECA) was isolated and its branches were occluded with an electrocoagulator at a point close to its origin. Following this, the origins of internal carotid artery (ICA) and pterygoparatine artery (PA) were exposed. After the CCA, ICA, and PA had been clipped, a 7–0 round tip nylon suture was introduced into the ICA via the ECA, advanced 8–10 mm distal to the carotid bifurcation and occluded MCA. At 1 h after ischemia, the mice were reanesthetized and the suture was withdrawn through ECA. Animals that were not showing grade 1 neurological symptoms, i.e. the failure to extend right forepaw (Hara et al., 1996), 1 h after ischemia, or those that developed hemorrhage, were excluded from the experiment on the basis of technical error.

2.3. Immunohistochemistries

Mice, which had been subjected to transient middle cerebral artery occlusion (tMCAO), were anesthetized with sodium pentobarbital (50 mg/kg) and then perfused transcardially with 0.9% saline followed by 2% paraformaldehyde in 50 mM phosphate buffer. Brains were then removed, postfixed and cryoprotected in 20% sucrose. Sections were cut on a cryostat at a thickness of 8 μm.

For IL-1β immunostaining, sections were preincubated in 10% normal horse serum after endogenous peroxidase blocking by 0.3% H_2O_2 and incubated with a polyclonal goat anti-murine IL-1β primary antibody (1:200, R&D Systems, Minneapolis, MN). Sections were rinsed and incubated with biotinylated horse anti-goat IgG (1:200, Vector, Burlingame, CA). They were then incubated in an avidin–biotin complex solution (Vector) followed by diaminobenzidine (DAB; Vector) as a chromogen. Same procedures were used for IL-1 receptor I (IL-1RI) immunostaining except for the use of a 1:50 dilution of rat anti-mouse CD121a (IL-1 receptor, type I/p80) monoclonal antibody (BD PharMingen, San Diego, CA) as a primary antibody and goat anti-rat IgG (Vector) as a secondary antibody.

Double staining of IL-1β and different known cell markers was used to determine which cells were expressing IL-1β. After staining for IL-1β using Alexa 546-labeled donkey anti-goat IgG antibody (1:400, Molecular Probes, Eugene, OR) as a secondary antibody, the sections were then incubated with monoclonal rat anti-mouse CD11b antibody (1:500, Serotec, Oxford, UK), monoclonal mouse anti-glial fibrillary acidic protein (GFAP) antibody (1:500, Sigma, St. Louis, MI) and monoclonal mouse anti-microtubule associated protein 2 (MAP2) antibody (1:500, Sigma) used as a marker for microglia and macrophages, astroglia, and neuronal cell marker, respectively. Then, sections were incubated with Alexa 488-labeled goat anti-rat IgG antibody (1:400, Molecular Probes) and Alexa 488-labeled goat anti-mouse IgG antibody. These staining were carried out on sections obtained from the brains of 3–4 mice at each

point considered. Sections were observed with the aid of a fluorescence microscope (Olympus AX-70; Olympus, Tokyo, Japan).

For 3-NT immunohistochemical staining, the same procedures as IL-1β single staining were followed, except for the use of 10% normal goat serum, a polyclonal affinity-purified rabbit anti-nitrotyrosine antibody (1:500, Upstate Biotechnology, Lake Placid, NY) as a primary antibody, biotinylated goat anti-rabbit IgG (Vector) as a secondary antibody. A 50-fold concentration of 3-NT (Sigma) was used as a control by preabsorption of the primary antibody. Sections were counterstained with hematoxylin after the DAB reaction identified the cells. The numbers of dark brown-stained 3-NT immunopositive cells in four different brain areas (two areas of somatosensory cortex, and a area of piriform cortex and striatum in a coronal section from the bregma 1.10 to −0.22 mm) from each hemispheres in a section were counted. A size of area that counted the number of cells is 440 × 320 μm^2, and the data was shown as cell number per mm^2. Three to four mice were examined at each time point.

Double staining of 3-NT and MAP2 was followed the same procedure as the double straining for IL-1β and cell markers, except that Alexa 546-labeled goat anti-rabbit IgG antibody (1:400, Molecular Probes) was used as a secondary antibody for 3-NT antibody.

2.4. Measurement of brain infarct volume

Forty-eight hour after tMCAO, the brains were removed and were sliced into four 2-mm coronal sections using a mouse brain matrix. Brain slices were then stained with 2% 2,3,5-triphenyltetrazolium chloride (TTC; Wako, Tokyo, Japan) at 37 °C for 30 min (Bederson et al., 1986). Brain slices were photographed on the anterior surface of each section and the areas of infarction were delineated on the basis of the relative lack of staining in the ischemic slice. The infarct areas were measured using NIH Image software and the infarct volumes were calculated by integration of the infarct areas. In order to correct for the effect of edema, the ipsilateral hemisphere determination was made indirectly by subtracting the area of the contralateral hemisphere in each section.

2.5. Measurement of regional cerebral blood flow

Regional cerebral blood flow (rCBF) was measured with laser-Doppler flowmetry (LBF-III; Biomedical Science, Tokyo, Japan). Mice were fixed in a stereotaxic frame and the skull of the ipsilateral hemisphere carefully removed using a dental drill. With the aid of a surgical microscope, a fiber-optic probe was placed 0.5-mm above the duramater, 2-mm posterior to the bregma and 4-mm lateral to the midline on the hemisphere ipsilateral to that where the transient occlusion was to be made. That is, over the site supplied by the proximal segment of the MCA. After measurement of the rCBF baseline value, the mice were removed once form the stereotaxic frame and subjected ischemia as described above. Then, the animals were again fixed in the stereotaxic frame. Blood flow was measured every 10 min during MCAO and up to 30 min after reperfusion. Blood flow values were expressed as a percentage of the rCBF baseline (before ischemia) values.

2.6. RT-PCR and real-time PCR determination

Brains were removed from sham-operated controls (0 h), and at 3, 6, 24, and 48 h after tMCAO. The cortex and striatum regions of both hemispheres were immediately separated on ice and then snap frozen using liquid nitrogen. The samples were stored at −80 °C until assayed. Total mRNA was extracted using the acid phenol–guanidinium thiocianate method (Chomczynski and Sacchi, 1987).

Total RNA was subjected to reverse transcription-PCR (RT-PCR) analysis. cDNA was synthesized from RNA. Total RNA (1.0 μg), random hexamer (Applied Biosystems, Foster City, CA) and manufacturer's recommended buffer were mixed and incubated at 95 °C for 2 min, then cooled to 37 °C, followed by incubation at 42 °C for 50 min with Superscript II (Invitrogen, Carlsbad, CA), 10 mM dithiothreitol, 0.5 mM each of dNTP mixture, and 20 U RNAsin (Promega, Madison, WI). PCR amplification of cDNA with primers specific for three different mouse NOS subtypes (neuronal NOS; nNOS, iNOS, and endothelial NOS; eNOS) and GAPDH as a house-keeping gene was carried out. The primer sequences for PCR and each PCR conditioning are shown in Table 1. DNA fragments of the three NOS subtypes and GAPDH were amplified as follows: 95 °C for 1 min, then each number of cycles (shown in Table 1) for 30 sec, and 72 °C for 1 min. The number of cycles ensuring non-saturating PCR conditions was established in preliminary experiments. PCR products were analyzed by electrophoresis on a 2% agarose gel containing ethidium bromide. Distilled water was used as negative control. Because of the cDNA was amplified as single and anticipation band using our setting primer, the cDNA was applied the real-time PCR to quantify the expression of NOS mRNA as follows.

NOS mRNA in tissues was quantified with real-time PCR using LightCycler (Roche, Mannheim, Germany) and Faststart Sybergreen I DNA quantification kits (Roche). cDNA was prepared as indicated above. Primers used for the analysis were the same as those described above. For the analysis of neuronal and endothelial NOS, and GAPDH, 2 μl of 20 μl RT reaction mixtures were applied to the LightCycler and amplified as follows: 95 °C for 10 min, then cycles of

Table 1
Primers, and conditions for PCR and LightCycler

Gene	Stand	Size (bp)	Sequence	PCR		LightCycler		
				Annealing (°C)	Cycles	Annealing (°C)	Cycles	$MgCl_2$ (mM)
nNOS	F	288	ATGTACAGGACGTGCTGCAG	65	40	65	40	4
	R		CTTCAATGAAGGCGATGGAC					
iNOS	F	200	AATACAAGATGACCCTAAGA	55	37			
	R		ACTTGCAAGTGAAATCCGAT					
eNOS	F	206	TGAGCAAGGACATATGTTTG	65	40	65	40	4
	R		TGCGTATGCGGCTTGTCACC					
GAPDH	F	253	AATGTGTCCGTCGTGGATCT	55	30	55	30	3
	R		TGTTGCTGTAGCCGTATTCA					

The mouse nNOS primers were corresponding to positions 4063–4082 and 4331–4350, respectively, of published mouse nNOS mRNA sequence (GenBank accession number MN008712). For the mouse iNOS, primers were corresponding to positions 301–320 and 481–500, respectively, (NM010927). The primers for mouse eNOS were corresponding to positions 3322–3341 and 3508–3527, respectively, (MN008713). The mouse GAPDH primers were corresponding to positions 755–774 and 788–1007, respectively, (NM008084).

95 °C for 10 s, 55 or 65 °C for 5 s, and 72 °C for 10 s. The melting curve analysis was done for 95 °C for 0 s, 65 °C for 15 s, then up to 99 °C at a temperature transition rate of 0.1 °C/s. Quantification programs, which determined the relative amount of mRNA and a melting curve program, were obtained from Roche. All data were normalized to GAPDH and expressed relative to the sham-operation controls in the wild-type mouse.

For RT-PCR analysis of IL-1β mRNA, the extracted mRNA (0.5 μg) was assayed using a mouse IL-1β relative RT-PCR kit (Ambion, Austin, TX). PCR products underwent electrophoresis on 2.0% agarose gels and were visualized with SYBR Green (SYBR Green II RNA Gel Stain; Molecular Probes) staining. As an internal control, 18S ribosomal RNA of each sample was assayed.

2.7. Statistical analysis

All data are expressed as the mean ± S.E. Statistical comparisons were made using the Student's *t*-test for unpaired samples. $P < 0.05$ was considered statistically significant.

3. Results

3.1. Expression of IL-1β and IL-1RI

The expression of IL-1β after ischemia in the wild-type mice is shown in Fig. 1. Immunoreactivity for IL-1β was not detected in either hemisphere of control mice. Increases in IL-1β immunoreactivity were noted in the ipsilateral hemisphere at 6 h after tMCAO. IL-1β immunoreactivity was also strongly expressed in the perifocal ischemic zone in the cortex and striatum between 12 and 24 h. However, the level of immunoreactivity had decreased by 48 h after ischemia (Fig. 1F). IL-1β positive cells were rarely detected in the contralateral hemisphere (Fig. 1G). Expressions of IL-1β mRNA were not detected in 0 h, were induced in the ipsilateral hemisphere at 6 h, and were decreased at 24 h (Fig. 1K). The similar pattern occurred in contralateral hemisphere. However, the levels were lower than those in ipsilateral hemisphere. IL-1β immunopositive cells were identified using double staining techniques (Fig. 2). Immunoreactivities for IL-1β were co-localized with that for CD11b, but were not with GFAP and MAP2.

IL-1RI immunostaining after ischemia is shown in Fig. 3. A few IL-1RI-immunopositive cells were observed in controls section. IL-1RI immunoreactivities slightly noted at 6 h and progressively increased up to 96 h after tMCAO. The positive cells in the contralateral hemisphere had also increased slightly by 96 h after tMCAO. The positive cells were recognized in microvasculature and neuron-like cells.

3.2. Brain infarct volumes after ischemia

In preliminary experiments we found that approximately 15% of mice that were subjected to tMCAO did not display the expected neurological symptoms, or hemorrhaged after reperfusion. And, there was no significant difference in the mortality between the two groups at 48 h after tMCAO.

Forty-eight hour after tMCAO, the extent of infarct volumes were measured using TTC staining (Fig. 4). Representative images of the anterior surface of four TTC-stained coronal sections are shown in Fig. 4A. The infarct volume in IL-1 KO mice (35.7 ± 7.1 mm^3, $n = 12$) was significantly smaller than that of wild-type mice (63.1 ± 8.3 mm^3, $n = 13$, $P < 0.05$).

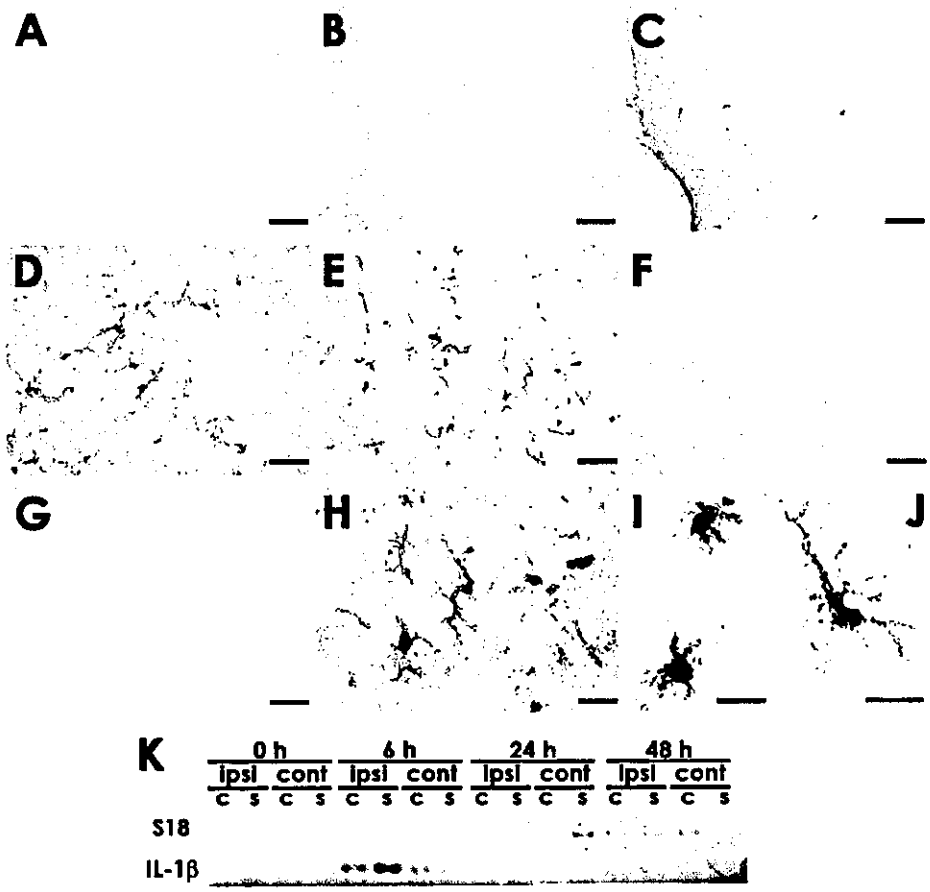

Fig. 1. Expression of IL-1β in wild-type mice after tMCAO. Photographs show results for sham-operated control mice (A) and animals studied 3 (B), 6 (C), 12 (D), 24 (E, H to J), and 48 (F) h after tMCAO in the cortex of the ipsilateral hemisphere. Cells immunopositive for IL-1β were noted slightly at 6 h (C), expressed strongly at 12 and 24 h (D and E), and decreased at 48 h (F) after tMCAO. At 24 h, expression was observed in the piriform cortex (H, and J) and striatum (I) of the perifocal area. Scale bar = 50 μm (A–G) and 20 μm (H–J). (K) The samples were prepared from the cortex (c) and striatum (s) of both hemispheres (ipsilateral, ipsi; contralateral, cont) from 0, 6, 24, 48 h after tMCAO. As an internal control, 18S ribosomal RNA was used.

3.3. Cerebral blood flow after ischemia

In order to exclude the possibility that gene disruptions could alter CBF after MCAO, thereby influencing the results, we measured rCBF in separate sets of wild-type and IL-1 KO animals ($n = 5$ in each group, Fig. 5). rCBF was found to undergo a reduction immediately after MCAO of approximately 20% of the baseline level. This reduction was sustained during 60 min of ischemia. After reperfusion, rCBF increased to a level ranging from 87 to 115% of baseline. There was no significant difference in rCBF between the two groups during the experimental period.

3.4. 3-NT immunohistochemistry

As shown in Fig. 6, there were few 3-NT-immunopositive cells in either the sham-operated mice or in the contralateral hemisphere of the experimental animals after tMCAO. 3-NT immunoreactivities were clearly observed in the ipsilateral hemisphere of the wild-type mice, with strong expression 24 h after tMCAO, decreasing slightly at 48 h. The immunopositive cells of 3-NT were identified in neurons because the cells co-expressed with MAP2 immunoreactivities (Fig. 7). The 3-NT immunoreactivities in neurons were observed in both cytoplasm and nucleus (Fig. 6B and C Fig. 7). The positive reactions were also often noted in the microvasculature (Fig. 6D). 3-NT -immunopositive cells in IL-1 KO mice displayed weaker expression (Fig. 6E and F). The number of 3-NT-immunopositive cells summarized in Fig. 8. There was no significant difference between the two groups in the ipsilateral hemisphere at 0 h, not in the contralateral hemisphere during the experiment. In ipsilateral hemisphere, the numbers of 3-NT-positive cells were markedly increased in wild-type mice (1556 ± 68 cells/mm^2) 24 h after tMCAO and were significantly less in IL-1 KO mice (728 ± 28, $P < 0.001$). The number of 3-NT-positive cells in the ipsilateral hemisphere of wild-type mice was seemingly decreased

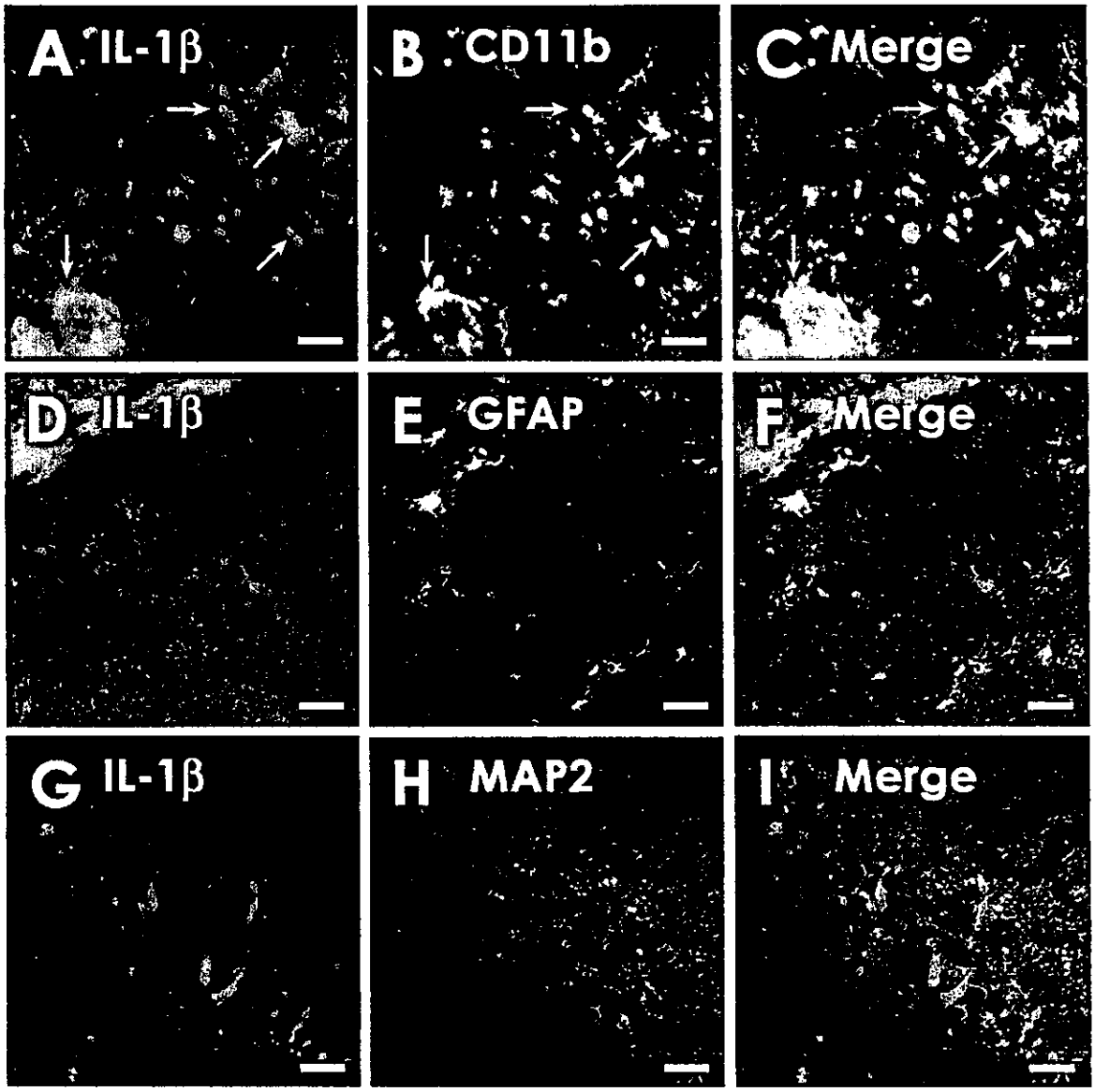

Fig. 2. Immunoreactivity for IL-1β is localized in the microglia and macrophages, but not in the astroglia or neurons 24 h after tMCAO. Double immunofluorescence staining was performed with IL-1β, and CD11b (A, B, and C), GFAP (D, E, and F), or MAP2 (G, H, and I) antibodies. Scale bar = 20 μm.

by 48 h after tMCAO such that there was no significant difference between these mice and the IL-1 KO mice. However, in wild-type mice, at 48 h after tMCAO, these sections had undergone shrinkage of the nuclei along with vacuolation and spongy degeneration of the parenchyma (Fig. 6C). Immunoreactivities for 3-NT were abolished by preabsorption with a 50-fold concentration of 3-NT (Fig. 6G and H).

3.5. Expression of mRNA for different NOS subtypes

It is considered that the immunostaining of 3-NT is a marker of $ONOO^-$ generation and that $ONOO^-$ is an oxidative product of the reaction between NO and O_2^-. We subsequently assessed whether IL-1 could be implicated in expression of mRNA for NOS after tMCAO (Fig. 9). After tMCAO, the expression of nNOS mRNA of wild-type mice had increased approximately 2-fold of 0 h (sham-operated control) within 3 h, and was found to decrease at the later times of 24 and 48 h. In sham-operated controls, nNOS mRNA in IL-1 KO mice was expressed at a lower level than that measured in wild-type mice. The mRNA expression had remarkably increased at 24–48 h. The expression of iNOS mRNA in wild-type mice increased progressively up to 48 h after ischemia. Although expression of iNOS mRNA in IL-1 KO mice was slightly decreased at 3 h and increased again at 24 h and then continuously up to 48 h, the levels

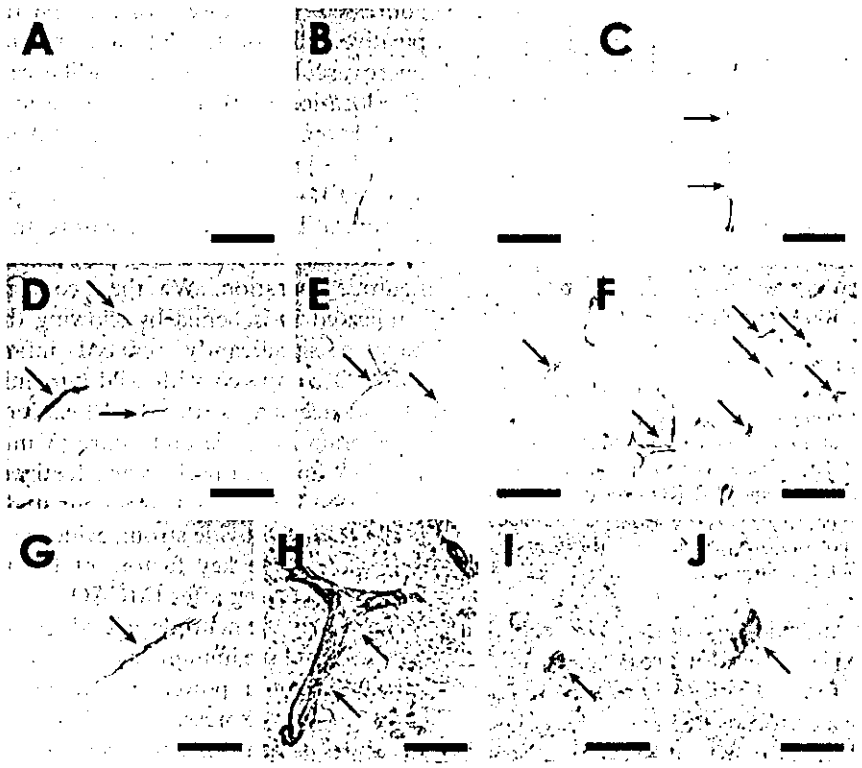

Fig. 3. Expressions of IL-1RI immunoreactivities in wild-type mice after tMCAO. Photographs show results for 0 (A), 6 (B), 12 (C), 24 (D, I), 48 (E, J), and 96 (F, G) h after tMCAO in the cortex of the ipsilateral (A–F, H–J) and the contralateral (G) hemisphere. Cells immunoreactivities for IL-1RI after tMCAO were narrowly noted at 6–12 h (B, C), increased progressively, 24–96 h (D, E, F). In the contralateral hemisphere, the immunopositive cells for IL-1RI increased slightly 96 h (G) after tMCAO. The morphological features of the cells immunopositive for IL-1RI were mainly associated with microvasculature (H; 96 h) and neuron-like cells (I; 24 h, J; 48 h). Scale bar = 100 μm (A–G) and 20 μm (H–J).

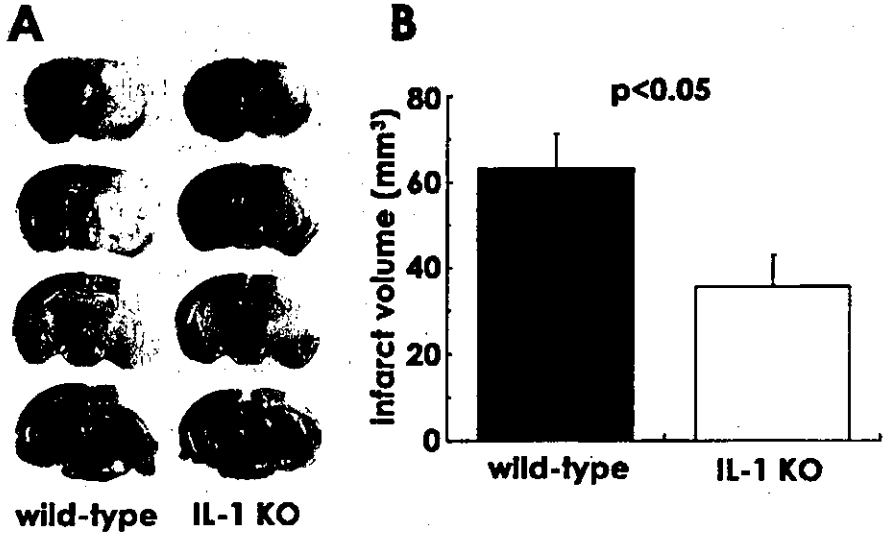

Fig. 4. Brain infarct volume 48 h after tMCAO in wild-type and IL-1 KO mice. (A) Representative images of the four TTC-stained 2-mm coronal sections analyzed for injury volumes in wild-type (left) and IL-1 KO (right) mice. The infarct regions appear as white areas. (B) Brain infarct volumes 48 h after tMCAO. Infarct volume of IL-1 KO mice ($n = 12$) was significantly decreased by comparison with that of wild-type mice ($n = 13$; $P < 0.05$) with the Student's t-test. Each value is the mean ± S.E.

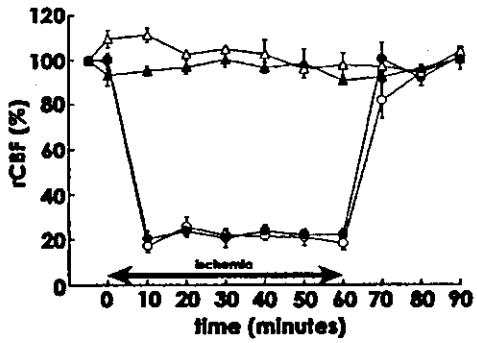

Fig. 5. rCBF during 60 min of MCAO and 30 min after reperfusion in the wild-type and IL-1 KO mice. rCBF was measured with laser-Doppler flowmetry using a fiber-optic probe placed 2-mm posterior to the bregma and 4-mm lateral to the midline on the hemisphere ipsilateral to the occlusion. There were no significant differences between the wild-type (circle: $n = 5$), and IL-1 KO mice (filled circle: $n = 5$). Sham-operated wild-type (triangle: $n = 3$) and IL-1 KO (filled triangle: $n = 3$) controls did not show any significant changes during the experiment. Each value is the mean ± S.E.

were lower than that in wild-type mice. The eNOS mRNA for wild-type mice showed a prominent 5-fold increase at 24 h after tMCAO and then rose continuously to give a 10-fold increase by 48 h (Fig. 9C). The level of eNOS mRNA in IL-1 KO mice was seldom altered by tMCAO.

4. Discussion

A number of previous reports have implicated IL-1 in the neurodegeneration associated with ischemic insult. However, the mechanisms underlying this are not well understood. For this reason, we sought to clarify the effects of IL-1 and the basis of its role in neurodegeneration using IL-1 KO mice. The expressions of IL-1β were noted several hours after ischemia and the proteins were strongest in the perifocal area at 24 h after tMCAO. Previous reports have suggested the involvement of endothelial cells, microglia, macrophages and astrocytes after ischemic and excitotoxic damage (Zhang et al., 1998; Hillhouse et al., 1998; Davies et al., 1999; Pearson et al., 1999; Imaizumi et al., 2001). However, in this study, the expression cells of IL-1β were only co-localized with microglia/macrophages, but not in astroglia and neuronal cells.

On the other hand, we determined the expression of IL-1RI after ischemia. There are two receptor types, IL-1RI and RII that can interact with IL-1α and β, with IL-1 believed to exert all of its actions by binding to IL-1RI (Dinarello, 1996; Basu et al., 2002). The induction of IL-1RI after global ischemia in rat was shown in the glia, neurons and sporadic microvascular endothelia (Sairanen et al., 1997). However, the localization of IL-1RI after focal ischemia in the mouse has yet to be addressed. We showed for the first time that immunopositive cells for IL-1RI were increased expression in microvasculature and neuron-like cells after ischemia. The location of IL-1RI was consistent with the infarct area. From these results, we postulated that the generated IL-1 in microglia/macrophages was secreted. Then, secreted IL-1 binds its signaling receptor IL-1RI, which is induced in the microvasculature and neuron-like cells of ischemic areas, and may play a role in the process of neurodegeneration. We then confirmed that IL-1 is implicated in ischemia by showing that IL-1 KO mice have a significantly reduced infarct volume after tMCAO compared with wild-type mice. Several pieces of evidence suggest that IL-1β exacerbates brain injury after brain ischemia and injury (Yamasaki et al., 1995; Loddick and Rothwell, 1996; Rothwell, 1999; Touzani et al., 1999). The results from our study along with these other studies provide strong evidence that expressed IL-1 is one of the key factors of the neurodegeneration process occurring after tMCAO.

To clearly the neurodegenerative mechanisms of IL-1, we examined the immunostaining for 3-NT, an oxidative metabolite of a powerful oxidant $ONOO^-$, in both mice. Strong expression of 3-NT after tMCAO was observed in neurons and microvasculature, which cells correspond to IL-1RI expression and the numbers of 3-NT-immunopositive cells in IL-1 KO mice were significantly lower than in wild-type mice. In these results, it is suggested that IL-1 generate the $ONOO^-$ and increase oxidative stress. However, there is no evidence that IL-1 directly is generated $ONOO^-$. Previous studies using cultured cells have indicated that the release of NO is related to the effect of IL-1β. Application of IL-1β to cultured rat brain endothelial cells, human fetal glial cells, and hippocampal neurons promotes the expression of iNOS mRNA and increases the release of NO (Bonmann et al., 1997; Ding et al., 1997; Serou et al., 1999; Trajkovic et al., 2001). Homma et al. (1997) used immunohistochemical techniques to show that three NOS subtypes were increased at different time points in the ipsilateral hemisphere after permanent ischemia in the rat brain. Mice that were deficient in nNOS and iNOS had a decreased brain infarct size after permanent or transient focal (Huang et al., 1994; Hara et al., 1996; Iadecola et al., 1997; Loihl et al., 1999; Nagayama et al., 1999; Elibol et al., 2001) and global (Panahian et al., 1996) ischemia. Moreover, we have reported in previous study that the immunoreactivities of iNOS in the IL-1 KO mice were weaker than that of wild-type mice in the hippocampus following forebrain ischemia, and that NO levels of IL-1 KO mice were lower than those in wild-type mice (Mizushima et al., 2002).

Therefore, we determined whether IL-1 influences the NOS expression after tMCAO. The expression of iNOS mRNA in IL-1 KO mice was down-regulated after

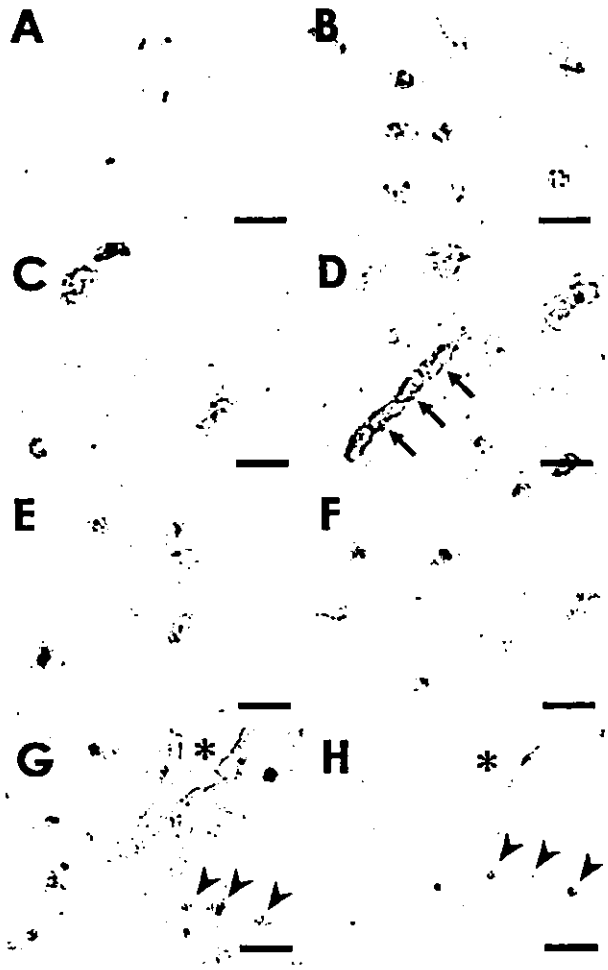

Fig 6

Fig. 7

Fig. 6. Expression of 3-NT immunoreactivity in the ipsilateral hemisphere after tMCAO. Photographs show the ipsilateral cortex in the wild-type (A–D, G and H) and IL-1 KO (E and F) mice 0 (A), 24 (B and E) and 48 (C, D, and F) h after tMCAO. Immunoreactivity for 3-NT was expressed strongly 24 (B) to 48 (C) h after tMCAO in neurons and was sometimes noted in vessels (D, arrows) of the wild-type mice. 3-NT positive cells were rare, and only weakly expressed, 24 (E) to 48 (F) h after tMCAO in IL-1 KO mice. (G) Cells immunopositive for 3-NT (arrowheads) can be noted in this section, whereas (H) these positive reactions were blocked with a 50-fold concentration of 3-NT in the consecutive section from the same brain. Blood vessels (asterisks) were used as markers to locate equivalent areas in the two sections. Scale bar = 10 μm (A–F) and 20 μm (G and H).

Fig. 7. Immunoreactivities for 3-NT are expressed in the neurons at 24 h after tMCAO. Double immunofluorescence staining was performed with 3-NT, and MAP2 antibodies. The immunoreactivities for 3-NT were highly observed in both cytoplasm (*yellow in Merge*) and nucleus (*red in Merge*). Scale bar = 20 μm.

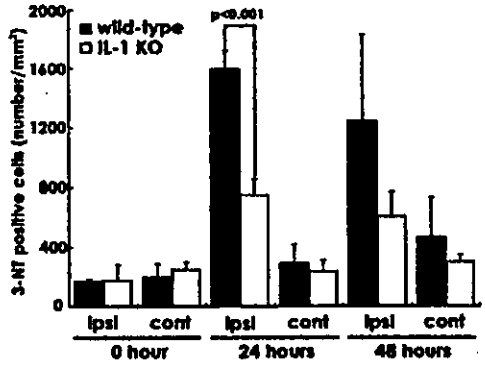

Fig. 8. 3-NT-immunopositive cells in the ischemic brain of wild-type and IL-1 KO mice. For each animal, the number of immunopositive cells across a section was counted in each hemisphere and calculated. There were few 3-NT-immunopositive cells in either the sham-operated mice (0 h) or in the contralateral hemisphere (cont) of the experimental animals. The 3-NT-positive cells in the ipsilateral hemisphere (ipsi) increased with time, peaking at 24 h then decreasing by 48 h after tMCAO. The number of 3-NT-positive cells in the ipsilateral hemisphere of the wild-type mice was significantly greater than that measured in IL-1 KO mice 24 h after tMCAO ($P < 0.001$). Each value is the mean ± S.E. (n, 3–4 mice in each group).

tMCAO and the expression of nNOS in the early stages, and eNOS were also dramatically decreased in IL-1 KO mice compared to wild-type mice. Conversely, the expression of nNOS mRNA in IL-1 KO was unexpectedly increased at 48 h after tMCAO in spite of decreasing for the 3-NT levels. Recently, it is reported that sustained and long-lasting inhibition of NOS aggravated the excitotoxic brain damage (Ciani et al., 2001), and that nNOS up-regulated the neuroprotective factor such as cAMP-responsive element binding protein and Bcl-2 in cerebellar culture neuron (Ciani et al., 2002). The nNOS expression in the later stage in IL-1 KO might be implicated in the role of neuroprotection. In general, it is considered that eNOS decreases neurodegenerative processes via dilation of the microvasculature during ischemia. Even partial inhibition of eNOS activity can result in large changes in rCBF and cause neuronal cell damage (Huang et al., 1994; Samdami et al., 1997; Bolaños and Almeida 1999). In present results, although the expression of eNOS mRNA in IL-1 KO mice was lower than in wild-type mice, the infarct volume of IL-1 KO mice after tMCAO was smaller than that of wild-type mice. It is possible that eNOS also participate in deterioration of infarction and the generation of $ONOO^-$ as to an environmental.

The expressions of NOS mRNA were not always consistent with expression of IL-1β and its receptor. IL-1α was not examined in this experiment. It has been reported that IL-1α mRNA were expressed continuously in brain and induced after ischemia (Horai et al., 1998; Boutin et al., 2001). Recently, Boutin et al. (2001) reported that IL-1β as well as IL-1α plays important roles in ischemic neuronal damage in IL-1α, β, and α/β KO mice. These results including us suggested that the expressions of NOS mRNA may be regulated by both IL-1 subtypes, not only IL-1β. It surely calls for further investigation for IL-1 and NOS expression.

Previous reports have implicated other roles for IL-1 in tissue damage. One is that a free radical inducer, cyclooxygenase-2 is induced by IL-1β during inflammatory periods in hippocampal neuronal cultures (Serou et al., 1999; Samad et al., 2001). IL-1 may be also participates in the expression of intercellular adhesion molecule-1 (ICAM-1). Following transfection with IL-

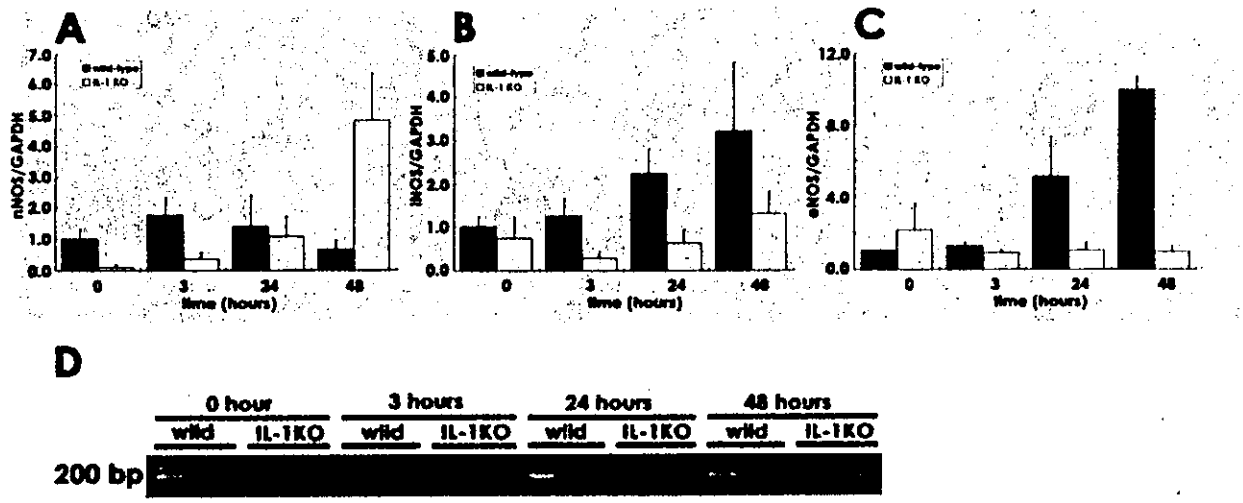

Fig. 9. Time-dependent comparison of expression of different subtypes of NOS mRNA in the ipsilateral cortex after tMCAO. The mRNA levels of nNOS (A) and eNOS (C) were quantified with the LightCycler and the level of iNOS mRNA (B) was determined by semi-quantitative RT-PCR. Representative scanned images of the iNOS mRNA in wild-type and IL-1 KO mice are shown in (D). All data were normalized to the mRNA of GAPDH and each value is shown as the mean ± S.E. (n, 3–4 mice for each time point). *: $P < 0.05$, **: $P < 0.01$ compared with the wild-type mice (Student's t-test).

1ra, immunostaining for ICAM-1 decreases after transient focal ischemia in mice (Yang et al., 1999a,b). The action of ICAM-1 on the endothelium is thought to facilitate the migration and infiltration of leukocytes, one of the major producers of O_2^- and NO into the ischemic brain (Matsuo et al., 1994; Kitagawa et al., 1998; Parmentier et al., 2000).

The effect of IL-1 might also involve the induction of delayed neuronal cell death such as apoptosis. Endogenous IL-1β plays an important role in hypoxia-mediated apoptosis in cultured cells (Friedlander et al., 1996). We have also demonstrated that, after global ischemia, the number of TUNEL-positive cells in hippocampus of wild-type mice increases with time in comparison with that in IL-1 KO mice (Mizushima et al., 2002).

In conclusion, IL-1 KO mice have significantly reduced brain injury after tMCAO as compared with wild-type mice. One of the mechanisms underlying this is the induced oxidative stress brought about by the release of an oxidative substance, $ONOO^-$, perhaps via the regulation of NOS.

Acknowledgements

This study was supported in part by grants from the Ministry of Education, Science, Sports and Culture (S.S.), and a High-Technology Research Center Project from the Ministry of Education, Science, Sports and Culture of Japan (H.O. and S.S.).

References

Basu, A., Krady, J.K., O'Malley, M., Styren, S.D., DeKosky, S.T., Levison, S.W., 2002. The type 1 interleukin-1 receptor is essential for the efficient activation of microglia and the induction of multiple proinflammatory mediators in response to brain injury. J. Neurosci. 21, 6071–6082.

Bederson, J.B., Pitts, L.H., Germano, S.M., Nishimura, M.C., Davis, R.L., Bartkowski, H.M., 1986. Evaluation of 2,3,5-triphenyltetrazolium chloride as a stain for detection and quantification of experimental cerebral infarction in rats. Stroke 17, 1304–1308.

Betz, A.L., Yang, G.-Y., Davidson, B.L., 1995. Attenuation of stroke size in rats using an adenoviral vector to induce overexpression of interleukin-1 receptor antagonist in brain. J. Cereb. Blood Flow Metab. 15, 550–551.

Bolaños, J.P., Almeida, A., 1999. Role of nitric oxide in brain hypoxia–ischemia. Biochim. Biophys. Acta 1411, 415–436.

Bonmann, E., Suschek, C., Spranger, M., Kolb-Bachofen, V., 1997. The dominant role of exogenous or endogenous interleukin-1 beta on expression and activity of inducible nitric oxide synthase in rat microvascular brain endothelial cells. Neurosci. Lett. 230, 109–112.

Boutin, H., LeFeuvre, R.A., Horai, R., Asano, M., Iwakura, Y., Rothwell, N.J., 2001. Role of IL-1α and IL-1β in ischemic brain damage. J. Neurosci. 21, 5528–5534.

Chomczynski, P., Sacchi, N., 1987. Single-step method of RNA isolation by acid guanidium thiocyanate–phenol–chloroform extraction. Anal. Biochem. 162, 156–159.

Ciani, E., Baldinotti, I., Contestabile, A., 2001. Sustained, long-lasting inhibition of nitric oxide synthase aggravates the neural damage in some models of excitotoxic brain injury. Brain Res. Bull. 56, 29–35.

Ciani, E., Guidi, S., Bartesaghi, R., Contestabile, A., 2002. Nitric oxide regulates cGMP-dependent cAMP-responsive element binding protein phosphorylation and Bcl-2 expression in cerebellar neurons: implication for a survival role of nitric oxide. J. Neurochem. 82, 1282–1289.

Davies, C.A., Loddick, S.A., Toulmond, S., Stroemer, R.P., Hunt, J., Rothwell, N.J., 1999. The progression and topographic distribution of interleukin-1β expression after permanent middle cerebral artery occlusion in the rat. J. Cereb. Blood Flow Metab. 19, 87–98.

D'Eutachio, P., Jadidi, S., Fuhlbrigge, R.C., Gray, P.W., Chaplin, D.D., 1987. Interleukin-1α and β genes: linkage on chromosome 2 in the mouse. Immunogenetics 26, 339–343.

Dinarello, C.A., 1996. Biologic basis for interleukin-1 in disease. Blood 87, 2095–2147.

Ding, M., St. Pierre, B.A., Parkinson, J.F., Medberry, P., Wong, J.L., Rogers, N.E., Ignarro, L.J., Merrill, J.E., 1997. Inducible nitric-oxide synthase and nitric oxide production in human fetal astrocytes and microglia. J. Biol. Chem. 272, 11327–11335.

Durum, S.K., Oppenheim, J.J., 1993. Proinflammatory cytokines and immunity. In: Paul, W.E. (Ed.), Fundamental Immunology, third ed.. Raven Press Ltd, New York, pp. 801–835.

Elibol, B., Soylemezoglu, F., Unal, I., Fujii, M., Hirt, L., Huang, P.L., Moskowitz, M.A., Dalkara, T., 2001. Nitric oxide is involved in ischemia-induced apoptosis in brain: a study in neuronal nitric oxide synthase null mice. Neuroscience 105, 79–86.

Friedlander, R.M., Gagliardini, V., Rotello, R.J., Yuan, J., 1996. Functional role of interleukin 1β (IL-1β) in IL-1β-converting enzyme-mediated apoptosis. J. Exp. Med. 184, 717–724.

Fukuyama, N., Takizawa, S., Ishida, H., Hoshiai, K., Shinohara, Y., Nakazawa, H., 1998. Peroxynitrite formation in focal cerebral ischemia-reperfusion in rats occurs predominantly in the peri-infarct region. J. Cereb. Blood Flow Metab. 18, 123–129.

Garcia, J.H., Liu, K.-F., Relton, J.K., 1995. Interleukin-1 receptor antagonist decreases the number of necrotic neurons in rats with middle cerebral artery occlusion. Am. J. Pathol. 147, 1477–1486.

Hara, H., Huang, P.L., Panahian, N., Fishman, M.C., Moskowitz, M.A., 1996. Reduced brain edema and infarction volume in mice lacking the neuronal isoform of nitric oxide synthase after transient MCA occlusion. J. Cereb. Blood Flow Metab. 16, 605–611.

Hillhouse, E.W., Kida, S., Iannotti, F., 1998. Middle cerebral artery occlusion in the rat causes a biphasic production of immunoreactive interleukin-1β in the cerebral cortex. Neurosci. Lett. 249, 177–179.

Homma, H., Mizushima, H., Arai, Y., Dohi, K., Matsumoto, K., Shioda, S., Nakai, Y., 1997. Effect of focal cerebral ischemia on nitric oxide synthase expression in rats. Med. Electron Microsc. 30, 55–62.

Horai, R., Asano, M., Sudo, K., Kanuka, H., Suzuki, M., Nishihara, M., Takahashi, M., Iwakura, Y., 1998. Production of mice deficient in genes for interleukin (IL)-1α, IL-1β, IL-1α/β, and IL-1 receptor antagonist shows that IL-1β is crucial in turpentine-induced fever development and glucocorticoid secretion. J. Exp. Med. 187, 1463–1475.

Huang, Z., Huang, P.L., Panahian, N., Dalkara, T., Fishman, M.C., Moskowitz, M.A., 1994. Effect of cerebral ischemia in mice deficient in neuronal nitric oxide synthase. Science 265, 1883–1885.

Iadecola, C., 1997. Bright and dark sides of nitric oxide in ischemic brain injury. Trends Neurosci. 20, 132–139.

Iadecola, C., Zhang, F., Casey, R., Nagayama, M., Ross, M.E., 1997. Delayed reduction of ischemic brain injury and neurological

deficits in mice lacking the inducible nitric oxide synthase gene. J. Neurosci. 17, 9157–9164.

Imaizumi, Y., Mizushima, H., Matsumoto, H., Dohi, K., Matsumoto, K., Ohtaki, H., Funahashi, H., Matsunaga, S., Horai, R., Asano, M., Iwakura, Y., Shioda, S., 2001. Increased expression of interleukin-1β in mouse hippocampus after global ischemia. Acta Histochem. Cytochem. 34, 357–362.

Kamii, H., Mikawa, S., Murakami, K., Kinouchi, H., Yoshimoto, T., Reola, L., Carlson, E., Epstein, C.J., Chan, P.H., 1996. Effects of nitric oxide synthase inhibition on brain infarction in SOD-1-transgenic mice following transient focal cerebral ischemia. J. Cereb. Blood Flow Metab. 16, 1153–1157.

Kitagawa, K., Matsumoto, M., Mabuchi, T., Yagita, Y., Ohtsuki, T., Hori, M., Yanagihara, T., 1998. Deficiency of intercellular adhesion molecule 1 attenuates microcirculatory disturbance and infarction size in focal cerebral ischemia. J. Cereb. Blood Flow Metab. 18, 1336–1345.

Loddick, S.A., Rothwell, N.J., 1996. Neuroprotective effects of human recombinant interleukin-1 receptor antagonist in focal cerebral ischaemia in the rat. J. Cereb. Blood Flow Metab. 16, 932–940.

Loihl, A.K., Asensio, V., Campbell, I.L., Murphy, S., 1999. Expression of nitric oxide synthase (NOS)-2 following permanent focal ischemia and the role of nitric oxide in infarct generation in male, female and NOS-2 gene-deficient mice. Brain Res. 830, 155–164.

Matsuo, Y., Onodera, H., Shiga, Y., Nakamura, M., Ninomiya, M., Kihara, T., Kogure, K., 1994. Correlation between myeloperoxidase-quantified neutrophil accumulation and ischemic brain injury in the rat. Effect of neutrophil depletion. Stroke 25, 1469–1475.

Mizushima, H., Zhou, C.J., Dohi, K., Horai, R., Asano, M., Iwakura, Y., Hirabayashi, T., Arata, S., Nakajo, S., Takaki, A., Ohtaki, H., Shioda, S., 2002. Reduced postischemic apoptosis in the hippocampus of mice deficient in interleukin-1. J. Comp. Neurol. 448, 203–216.

Nagayama, M., Aber, T., Nagayama, T., Ross, M.E., Iadecola, C., 1999. Age-dependent increase in ischemic brain injury in wild-type mice and in mice lacking the inducible nitric oxide synthase gene. J. Cereb. Blood Flow Metab. 19, 661–666.

Panahian, N., Yoshida, T., Huang, P.L., Hedley-Whyte, E.T., Dalkara, T., Fishman, M.C., Moskowitz, M.A., 1996. Attenuated hippocampal damage after global cerebral ischemia in mice mutant in neuronal nitric oxide synthase. Neuroscience 72, 343–354.

Parmentier, S.B., Margaill, I., Plotkine, M., 2000. Modulation by nitric oxide of cerebral neutrophil accumulation after transient focal ischemia in rats. J. Cereb. Blood Flow Metab. 20, 812–819.

Pearson, V.L., Rothwell, N.J., Toulmond, S., 1999. Excitotoxic brain damage in the rat induces interleukin-1β protein in microglia and astrocytes: correlation with the progression of cell death. Glia 25, 311–323.

Relton, J.K., Rothwell, N.J., 1992. Interleukin-1 receptor antagonist inhibits ischaemic and excitotoxic neuronal damage in the rat. Brain Res. Bull. 29, 243–246.

Rothwell, N.J., 1999. Cytokines-killers in the brain? J. Physiol. 514, 3–17.

Sairanen, T.R., Lindsberg, P.J., Brenner, M., Siren, A.-L., 1997. Global forebrain ischemia results in differential cellular expression of interleukin-1β (IL-1β) and its receptor at mRNA and protein level. J. Cereb. Blood Flow Metab. 17, 1107–1120.

Samad, T.A., Moore, K.A., Sapirstein, A., Billet, S., Allchorne, A., Poole, S., Bonventre, J.V., Woolf, C.J., 2001. Interleukin-1β-mediated induction of COX-2 in the CNS contributes to inflammatory pain hypersensitivity. Nature 410, 471–475.

Samdami, A.F., Dawson, T.M., Dawson, V.L., 1997. Nitric oxide synthase in models of focal ischemia. Stroke 28, 1283–1288.

Sanderson, K.L., Raghupathi, R., Saatman, K.E., Martin, D., Miller, G., McIntosh, T.K., 1999. Interleukin-1 receptor antagonist attenuates regional neuronal cell death and cognitive dysfunction after experimental brain injury. J. Cereb. Blood Flow Metab. 19, 1118–1125.

Serou, M.J., DeCoster, M.A., Bazan, N.G., 1999. Interleukin-1 beta activates expression of cyclooxygenase-2 and inducible nitric oxide synthase in primary hippocampal neuronal culture: platelet-activating factor as a preferential mediator of cyclooxygenase-2 expression. J. Neurosci. Res. 58, 593–598.

Silver, A.R.J., Masson, W.K., Geroge, A.M., Adam, J., Cox, R., 1990. The IL-1α and β genes are closely linked (< 70 kb) on mouse chromosome 2. Somatic Cell Mol. Genet. 16, 549–556.

Tanaka, K., Shirai, T., Nagata, E., Dembo, T., Fukuuchi, Y., 1997. Immunohistochemical detection of nitrotyrosine in postischemic cerebral cortex in gerbil. Neurosci. Lett. 235, 85–88.

Tocci, M.J., Schmidt, J.A., 1997. Interleukin-1: structure and function. In: Remick, D.G., Friedland, J.S. (Eds.), Cytokines in Health and Disease, second ed.. Marcel Decker Inc, New York, pp. 1–27.

Touzani, O., Boutin, H., Chuquet, J., Rothwell, N., 1999. Potential mechanisms of interleukin-1 involvement in cerebral ischaemia. J. Neuroimmunol. 100, 203–215.

Trajkovic, V., Stosic-Grujicic, S., Samardzic, T., Markovic, M., Miljkovic, D., Ramic, Z., Stojkovic, M.M., 2001. Interleukin-17 stimulates inducible nitric oxide synthase activation in rodent astrocytes. J. Neuroimmunol. 119, 183–191.

Van Dam, A.M., Bauer, J., Tilders, F.J.H., Berkenbosch, F., 1995. Endotoxin-induced appearance of immunoreactive interleukin-1β in ramified microglia in rat brain: a light and electron microscopic study. Neuroscience 65, 815–826.

Yamasaki, Y., Mastuura, N., Shozuhara, H., Onodera, H., Itoyama, Y., Kogure, K., 1995. Interleukin-1 as a pathogenetic mediator of ischemic brain damage in rats. Stroke 26, 676–681.

Yang, G.Y., Mao, Y., Zhou, L.F., Ye, W., Liu, X.H., Gong, C., Betz, A.L., 1999a. Attenuation of temporary focal cerebral ischemic injury in the mouse following transfection with interleukin-1 receptor antagonist. Brain Res. Mol. Brain Res. 72, 129–137.

Yang, G.Y., Schielke, G.P., Gong, C., Mao, Y., Ge, H.L., Liu, X.H., Betz, A.L., 1999b. Expression of tumor necrosis factor-alpha and intercellular adhesion molecule-1 after focal cerebral ischemia in interleukin-1β converting enzyme deficient mice. J. Cereb. Blood Flow Metab. 19, 1109–1117.

Zhang, Z., Chopp, M., Goussev, A., Powers, C., 1998. Cerebral vessels express interleukin 1β after cerebral ischemia. Brain Res. 784, 210–217.

European Journal of Neuroscience
Volume 17 Issue 5 Page 929 - March 2003
doi:10.1046/j.1460-9568.2003.02514.x

Aberrant responses to acoustic stimuli in mice deficient for neural recognition molecule NB-2

Hong Li[1], Yasuo Takeda[1], Hiroaki Niki[2], Junko Ogawa[1], Satoru Kobayashi[1], Nobuyuki Kai[2], Keiko Akasaka[1], Masahide Asano[3], Katsuko Sudo[4], Yoichiro Iwakura[4] and Kazutada Watanabe[1,5]

Abstract

NB-2, a member of the contactin subgroup in the immunoglobulin superfamily, is expressed specifically in the postnatal nervous system, reaching a maximum level at 3 weeks postnatal. NB-2 displays neurite outgrowth-promoting activity *in vitro*. To assess its function in the nervous system, we generated mutant mice in which a part of the NB-2 gene was ablated and replaced with the tau-LacZ gene. The general appearance of NB-2-deficient mice and their gross anatomical features were normal. The LacZ expression patterns in heterozygous mice revealed that NB-2 is preferentially expressed in the central auditory pathways. In the audiogenic seizure test, NB-2-deficient mice exhibited a lower incidence of wild running, but a higher mortality rate than the wild-type littermates. c-Fos immunohistochemistry demonstrated that neural excitability induced by the audiogenic seizure test in the NB-2-deficient mice was prominently attenuated in both the dorsal and external cortices of the inferior colliculus, where enhanced neural excitability was observed in the wild-type mice. In response to pure-tone stimulation after priming, NB-2-deficient mice exhibited a diffuse and low level of c-Fos expression in the central nucleus of the inferior colliculus, which was distinctly different from the band-like c-Fos expression corresponding to the tonotopic map in the wild-type littermates. Taken together, these results suggest that a lack of NB-2 causes impairment of the neuronal activity in the auditory system.

International Immunology, Vol. 15, No. 4, pp. 483–490
doi: 10.1093/intimm/dxg054

IL-1 is required for allergen-specific T_h2 cell activation and the development of airway hypersensitivity response

Susumu Nakae[1], Yutaka Komiyama[1], Hiroshi Yokoyama[1,4], Aya Nambu[1], Masaomi Umeda[3], Michiko Iwase[2], Ikuo Homma[2], Katsuko Sudo[1], Reiko Horai[1], Masahide Asano[1,5] and **Yoichiro Iwakura[1]**

[1]Center for Experimental Medicine, Institute of Medical Science, University of Tokyo, 4-6-1 Shirokanedai, Minato-ku, Tokyo 108-8639, Japan
[2]Second Department of Physiology, Showa University School of Medicine, 1-5-8 Hatanodai, Shinagawa-ku, Tokyo 142-8555, Japan
[3]Research Center Kyoto, Bayer Yakuhin, Ltd, 6-5-1-3 Kunimidai, Kizu-cho, Sorakugun, Kyoto 619-0216, Japan

[4]Present address: Department of Biophysics and Biochemistry, Graduate School of Science, University of Tokyo, 7-3-1 Hongo, Bunkyo-ku, Tokyo 113-0033, Japan
[5]Present address: Institute for Experimental Animals, School of Medicine, Kanazawa University, 13-1 Takaramachi, Kanazawa 920-8640, Japan

Keywords: IL-1 receptor antagonist, IL-1α, IL-1β, knockout mouse

Abstract

IL-1 is a pro-inflammatory cytokine consisted of two molecular species, IL-1α and IL-1β, and the IL-1 receptor antagonist (IL-1Ra) is a natural inhibitor of both molecules. Although it is suggested that IL-1 potentiates immune responses mediated by T_h2 cells, the role of IL-1 in asthma still remains unclear. In this study, we demonstrate that the ovalbumin (OVA)-induced airway hypersensitivity response (AHR) in IL-1α/β-deficient (IL-1α/β$^{-/-}$) mice was significantly reduced from the levels seen in wild-type mice, whereas the responses seen in IL-1Ra$^{-/-}$ mice were profoundly exacerbated, suggesting that IL-1 is required for T_h2 cell activation during AHR. OVA-specific T cell proliferation, IL-4 and IL-5 production by T cells, and IgG1 and IgE production by B cells in IL-1α/β$^{-/-}$ mice were markedly reduced compared with these responses in wild-type mice; such responses were enhanced in IL-1Ra$^{-/-}$ mice. Using IL-1α$^{-/-}$ and IL-1β$^{-/-}$ mice, we determined that both IL-1α and IL-1β are involved in this reaction. Both IgG1 and IgE levels were reduced in IL-1β$^{-/-}$ mice, while only IgE levels were affected in IL-1α$^{-/-}$ mice, indicating a functional difference between IL-1α and IL-1β. These observations indicate that IL-1 plays important roles in the development of AHR.

Introduction

Allergic asthma is a T_h2 cytokine-mediated inflammatory response of the lungs characterized by mucus hypersecretion, airway inflammation and airway hyper-responsiveness to spasmogenic stimuli (1). In cases of asthma presenting with lung inflammation, the infiltration of eosinophils is predominant; the degree of infiltration correlates with illness severity (2). T cells, B cells and mast cells are also involved in the development of the allergic response, acting through the release of cytokines, antibodies and inflammatory mediators (1,3).

Allergen-specific T_h2 cells function in the development of AHR by secreting cytokines, including IL-4, IL-5 and IL-13 (1). IL-4 and IL-13 are required for AHR induction through inducing allergen-specific IgG1 and IgE production (4), resulting in the activation of mast cells via antigen/antibody complex–Fc receptor signaling (5), while IL-5 demonstrates a critical role in eosinophilia (4,6). Activated mast cells produce IL-4, IL-5, tumor necrosis factor (TNF)-α and various inflammatory mediators within the inflammatory site (5). IL-4 and TNF-α can induce vascular cell adhesion molecule (VCAM)-1

Correspondence to: Y. Iwakura; E-mail: iwakura@ims.u-tokyo.ac.jp

Transmitting editor: S. J. Galli

Received 1 October 2002, *accepted* 8 January 2003

expression on endothelial cells, leading to the adhesion of various inflammatory cells to local inflammatory sites (7,8).

IL-1, a pro-inflammatory cytokine involved in a variety of immune responses, can promote mast cell activation and production of T_h2 cytokines (9,10), suggesting that IL-1 functions in the development of allergic diseases. It is also known that IL-1 is a potent inducer of VCAM-1 on vascular endothelial cells (11–13) and mice lacking the type I IL-1 receptor (IL-1RI$^{-/-}$ mice) exhibit reduced eosinophil recruitment into the lungs due to the decreased expression of VCAM-1 during antigen-induced AHR (14). Furthermore, IL-1 can activate T_h2 cells and enhance antibody production (15–20). The involvement of IL-1 in asthmatic diseases that are mediated by T_h2 cells, however, remains unclear. It is also unknown if either IL-1α or IL-1β or both are necessary for AHR development. In this study, we demonstrate that IL-1 is required for allergen-specific T_h2 cell activation and that both IL-1α and IL-1β function in the development of AHR.

Methods

Mice

IL-1α$^{-/-}$, IL-1β$^{-/-}$, IL-1α/β$^{-/-}$ and IL-1Ra$^{-/-}$ mice were generated by homologous recombination as described, then backcrossed to BALB/cA mice for eight generations (21). DO11.10 Tg mice (BALB/c background) were kindly provided by Dr Dennis Y. Loh (22). All mice were housed under specific pathogen-free conditions in an environmentally controlled clean room at the Center for Experimental Medicine, Institute of Medical Science, University of Tokyo. All experiments were conducted according to the institutional ethical guidelines for animal experiments and safety guidelines for gene manipulation. Sex- and age-matched adult mice aged 8–12 weeks old were used for experimentation.

Ovalbumin (OVA)/alum-induced airway hypersensitivity

Mice were actively sensitized by i.p. injection of 100 μg of OVA with aluminum potassium sulfate (alum) on days 0 and 14. They were challenged intranasally by 100 μg of OVA in 50 μl saline, using a microsyringe, on days 14, 21, 24 and 27. Sham-sensitized mice were treated with i.p. injections of alum precipitated with saline alone and intranasal doses of saline alone. Twenty-four hours after the last intranasal administration of OVA, mice were anesthetized with pentobarbital (80 mg/kg, i.p.) and i.v. access was established by cannulating the jugular vein. The trachea was cannulated and connected to a rodent ventilator (model 687; Harvard Apparatus, South Natick, MA) with air supplemented at a tidal volume of 100.8 ± 3.3 μl/10 g body wt (n = 24), frequency of 100 breaths/min and positive end-expiratory pressure of 3 cmH_2O. After neuromuscular blockade with gallamine triethiodide (10 mg/kg, i.v.), bronchoconstriction was measured according to the overflow method, using a pressure transducer (7020; Ugo Basile, Milan, Italy) connected to the tracheal cannula. To assess the bronchial responsiveness to i.v. injected acetylcholine (ACh), the changes in the respiratory overflow volume were measured using progressively increasing doses of ACh. The increase in respiratory overflow volume provoked by ACh was represented as a percentage of the maximal overflow volume (100%) obtained by clamping the tracheal cannula.

OVA/PBS-induced airway hypersensitivity

OVA immunization without alum was performed as described previously (23,24). Briefly, mice were i.p. injected with 10 μg of OVA (grade II; Sigma, St Louis, MO) in 0.5 ml of PBS on each of 7 alternate days (one injection per day). Four weeks after the final immunization, mice were challenged intranasally 8 times for 8 days (one challenge per day) with 20 μl of either PBS alone as a control or PBS containing 100 μg of OVA. AHR to methacholine was assessed using the parameter P_{enh} (enhanced pause), which is calculated automatically based on the mean pressure generated in plethysmograph chambers during inspiration and expiration with the Buxco system as described elsewhere (25). Twenty-four hours following the last inhalation of OVA, bronchial responses to aerosolized methacholine (Sigma) were measured using the Buxco system (Buxco Electronics, Sharon, CT).

OVA-specific T cell proliferation assay

To measure secondary T cell responses, submaxillary lymph nodes (LN) were harvested 24 h after the last challenge with OVA. Single-cell suspensions prepared from these samples were cultured in a 96-well flat-bottom plate at a concentration of 5 × 10^4 cells/well in the absence or presence of 40 μg/ml OVA for 72 h. The primary T cell response was measured using DO11.10 CD4$^+$ T cells as described previously (26). The CD4$^+$ T cells from DO11.10 Tg mice (5 × 10^5 cells/well) and Thy1.2$^-$B220$^-$ splenic adherent cells (1 × 10^4 cells/well) from either wild-type or IL-1-deficient mice were cultured in the absence or presence of 0.1 μM OVA323–339 peptide for 72 h. Next, [^{3}H]thymidine (0.25 μCi/ml) (Amersham, Little Chalfont, UK) was added to the culture. After a 6-h label, the cells were harvested using a Micro 96 cell harvester (Skatron, Lier, Norway). Incorporated [^{3}H]thymidine was measured using the Micro Beta System (Pharmacia Biotech, Piscataway, NJ).

Detection of cytokine by ELISA

The Mini Kit mouse IL-4 kit (Endogen, Woburn, MA) for IL-4 and Titer Zyme EIA kit (PerSeptive Diagnostics, Cambridge, MA) for IL-5 were used to determine the cytokine levels according to the manufacturer's protocol.

Detection of serum Ig

To detect either OVA-specific or total Ig levels by ELISA, 50 μl of either 10 μg/ml OVA or 10 μg/ml rabbit anti-mouse Ig (Dako, Glostrup, Denmark) was coated onto 96-well flat-bottom plates. Following blocking with 0.05% skim milk in PBS for 1 h, 50 μl of the test samples was added to each well. After extensive washing, 50 μl of either alkaline phosphatase–goat anti-mouse IgG1 (Zymed, San Francisco, CA) or alkaline phosphatase–rat anti-mouse IgE (Southern Biotechnology Associates, Birmingham AL) was added to visualize bound antibodies. Alkaline phosphatase activity was measured using Substrate Phosphatase SIGMA104 (Sigma).

Statistics

Student's t-test was used for the statistical evaluation of the results.